

# D2.4

## Novel testing procedures for tidal composite blades

**Lead Beneficiary** TECNALIA

**Delivery date** 2023-03-13

**Dissemination level** Public

**Status** Final

**Version** 5.0

**Keywords** Ageing, composite material, tidal blade, degradation



This project has received funding from the European Union's Horizon 2020 research and innovation programme under grant agreement No 815278.

[www.nemmo.eu](http://www.nemmo.eu)  [@NEMMO\\_Project](https://twitter.com/NEMMO_Project)  [info@nemmo.eu](mailto:info@nemmo.eu)

## Document Information

<b>Grant Agreement Number</b>	815278
<b>Project Acronym</b>	NEMMO
<b>Work Package</b>	2
<b>Task(s)</b>	2.4
<b>Deliverable</b>	D2.4
<b>Title</b>	Novel testing procedures for tidal composite blades
<b>Author(s)</b>	Jean-Baptiste Jorcin; Chloe Richards; Adrián Delgado Ollero; Philip Daly; Fiona Regan; Yan Delauré; Jan Hallander; Erik Steen Jensen
<b>File Name</b>	Deliverable NEMMO D2.4 v5.0

## Change Record

Revision	Date	Description	Reviewer
1.0	03-06-2021	Tecnalia contribution	Jean-Baptiste Jorcin
2.0	06-07-2021	DCU contribution	Jean-Baptiste Jorcin
3.0	28-10-2021	SSPA contribution	Jean-Baptiste Jorcin
4.0	22-10-2022	BLAEST contribution	Jean-Baptiste Jorcin
5.0	13-03-2023	Update BLAEST contribution	Jean-Baptiste Jorcin



## Table of contents

<b>Introduction.....</b>	<b>6</b>
<b>Task 2.4.1: definition of a tailored accelerated ageing test for composite material .....</b>	<b>7</b>
<b>State of the art on the degradation mechanism of composite in sea water .....</b>	<b>7</b>
Water absorption .....	7
Mechanical loads.....	8
Photo-oxidation (Solar UV) .....	8
Degradation mechanisms summary .....	8
<b>Ageing procedure.....</b>	<b>9</b>
Natural environment: HarshLab .....	9
Natural environment: Port of Pasaia .....	10
Accelerated ageing in laboratory.....	11
Ageing procedure summary .....	13
<b>Characterization of the materials and the aging process .....</b>	<b>14</b>
Physicochemical methods:.....	14
Mechanical methods .....	17
Optical methods .....	19
Material characterization summary.....	19
<b>Experimental campaigns .....</b>	<b>20</b>
Material .....	20
HarshLab: ageing and experimental issues.....	21
Pasaia Port .....	24
Accelerated ageing test: ageing and experimental issues .....	27
Summary of the experimental campaign .....	27
<b>Damage assessment and discussion .....</b>	<b>28</b>
Characterization .....	28
Discussion and recommendation for a novel test procedure .....	35
Summary of the damage assessment and discussion .....	35
<b>Conclusion .....</b>	<b>36</b>
<b>Task 2.4.2 Development of fouling test for tidal turbines composite blades in dynamic conditions in sea environments .....</b>	<b>37</b>

<b>Overview of test conditions and design approach.....</b>	<b>37</b>
<b>Detailed review of design.....</b>	<b>38</b>
Methodology.....	38
<b>Simulation results .....</b>	<b>40</b>
Test section dimensioning.....	46
<b>Best performing candidate anti-fouling surface and material solutions .....</b>	<b>47</b>
<b>Test Programme.....</b>	<b>47</b>
<b>Test Methodology.....</b>	<b>48</b>
Lowry assay.....	48
Anthrone-sulphuric acid assay for carbohydrate determination .....	48
Identification of diatom communities using scanning electron microscopy (SEM).....	49
<b>Task 2.4.3 Definition of a tailored accelerated wear test for composite tidal blades working under cavitation turbulence and laminar flow conditions ...</b>	<b>50</b>
<b>Task 2.4.4 Definition of an accurate dynamic test for fatigue evaluation of composite blades for tidal turbines.....</b>	<b>53</b>
Background information: .....	53
The NEMMO project idea: .....	54
<b>Bibliography .....</b>	<b>56</b>

## Introduction

This document reports the work conducted during the task 2.4 of the work package 2 of the NEMMO project. The overall goal of the NEMMO project is to improve blade of tidal turbine in composite material for tidal energy generation.

This specific work is focus on designing a testing and characterization protocol to assess the degradation suffered by the materials of these blades due to the exposition to the sea water environment.

Tidal turbines are a promising opportunity to exploit ocean current flows clean energy production. Fibre reinforced composites (FRC) are frequently used in offshore structures and the field of their application is constantly expanding. Employing FRC for tidal turbine blades offers potential improvements in hydrodynamic and structural performance. The reliability of these materials, in a very severe environment is crucial to the profitability of tidal current energy systems. These structures are subject to many forces such as ocean tides, waves, storms but also to various marine aggressions, such as corrosion and performance degradation due to the growth of biofouling.

In a first part, in order to assess the degradation of the NEMMO composite blade material, which consist in a glass fiber reinforced vinyl ester resin composites with a gelcoat surface finishing, a test procedure was setup made of an ageing protocol in natural and laboratory environments couple with characterization techniques for damage evaluation. The material that will be used in this work is the reference material already in use on the existing tidal generator (without the material improvement provided by the NEMMO project).

A second part will be focused on the development of techniques to study the biofouling behaviour in dynamic condition. A new dynamic device will be designed as well as biofouling detection protocol to assess the biofouling presence and evolution.

A third part focus on the choice of experimental protocol to perform cavitation artificial ageing on blade material and coating with a specific device called sonotrode.

Finally, the last part is dedicated to the development of realsize blade fatigue test.

### **Task 2.4.1: definition of a tailored accelerated ageing test for composite material**

Sea water ageing in the tidal turbine environment, at ocean temperature, will generate a slow process of degradation and damage in the composites[1]. The resulting degradation mechanisms are quite complex and usually dependent on the specific material and operating environment.

There are two main factors that will affect the service-life of a submerged composite. These include water absorption into the material and mechanical loads. Both factors are interrelated and directly influence the others. Additionally, the composite may be also exposed to solar UV radiation which enhances the polymer degradation. High pressure environments are also considered to affect the degradation of the composite as well as the presence of biofouling. The degradation considered here is “off-load”, meaning that the material is not submitted to an intentional constant or dynamic mechanical load that may end to mechanical failure due to overload or fatigue.

The NEMMO composite blade material (glass fiber reinforced vinyl ester resin composites with a gelcoat surface finishing) degradation assessment will be done with a test procedure developed in the frame of the project that consists in an ageing protocol in natural and laboratory environments coupled with characterization techniques for damage evaluation. The material that will be used in this work is the reference material already in use on the existing tidal generator (without the material improvement provided by the NEMMO project).

After a quick overview of the degradation mechanisms, the ageing procedure will be presented followed by a review of possible characterization methods for damage assessment. The results obtained during the experimental campaign will be then presented followed by recommendation for ageing procedure modification to apply in the WP4 where the material improved during the NEMMO project will be tested.

### **State of the art on the degradation mechanism of composite in sea water**

As mentioned earlier, the main mechanisms expected are linked to water absorption, that may affect the mechanical properties of the material and possible effect of UV light on the chemical structure of composite material.

#### **Water absorption**

The absorption of water molecules in polymer composites is known to have important effects on their final performance, especially in their long-term exploitation. Because of the organic nature of the matrix resin long immersion in sea water can induce both physical and chemical changes. Plasticization and swelling are the main physical consequences of water absorption on polymer structures. Plasticization corresponds to a modification of the structure of the polymer and results in a decrease of the glass transition temperature. It also induces loss of mechanical properties with a reduction in moduli and failure stress. Swelling of the matrix is caused by the penetration of water into polymers, consequently volume changes will occur. At the composite scale, swelling can create interfacial cracks and fibre/matrix debonding. Transverse cracking (intra-laminar) is the principal damage mechanism in unidirectional composite laminates loaded off-axis. A transverse crack is often followed by debonding at the plies interface. This micro-debonding can have a major influence on both transverse cracking saturation and on the composite out-of-plane-strength. As a result, the lifetime of composites will be dominated by their interlaminar or out-of-plane response.

When composites are immersed at sea, water is first absorbed at the surface and then diffuses into the material. Experimentally it is also possible to follow water concentration in polymer and composite materials. There are various experimental methods but the simplest and the most popular is based on gravimetric measurements of the sample during immersion.

The kinetics of diffusion can change during the service life of composites in operation, damage due to the diversity of mechanical loads may impact and accelerate the diffusion of water inside the composite structures, as damage can create new pathways for water entry.

### Mechanical loads

The mechanical loads onto the tidal turbine blades are determined by three main factors:

- Tidal currents, which induce the rotation which generates energy
- Rotation, with a pressure variation due to depth changes of up to 20 m
- Waves, which affect underwater structures in shallow depths[2].

It has been shown that the general effect of mechanical loading onto the composite material is to enhance the moisture-penetration mechanisms producing higher rates and maximum levels of moisture penetration. As a result, aging mechanisms taking place under the effect of moisture are also enhanced, thus decreasing the durability of the material[3]. More specifically, application of tensile stresses enhances moisture absorption in GFRP while compressive stresses reduce the water uptake. The change in the free volume fraction of the composite also affects the water absorption capacity of a composite. When the applied stress causes the decrease in the free volume fraction of the resin matrix of a composite, the equilibrium water content is reduced and vice versa[4].

### Photo-oxidation (Solar UV)

Photo-oxidative degradation is the process of decomposition of the material by the action of light, which is considered as one of the primary sources of damage exerted upon polymeric substrates at ambient conditions.

Depending on where the underwater electrical is installed (sea floor, surface...), it can be affected by UV light. According to [5], the penetration of UV is depending to the turbidity of the water. For a high turbidity, it is possible to measure 10% of the surface UV at 3m underwater, but it shifts to 13m for a low turbidity.

Most of the synthetic polymers are susceptible to degradation initiated by UV and visible light. Normally the near-UV radiations (290-400 nm) in the sunlight determine the lifetime of polymeric materials in outdoor applications[6], [7]. Usually, the groups the most sensitive to UV are ester, then aldehyde, formate, and propyl end groups[8].

### Degradation mechanisms summary

*The main expected degradation mechanisms for composite material such as glass fiber reinforced vinyl ester composite in sea water environment are the synergy between water absorption and the natural mechanical load (waves, sea current) and the photo-oxidation*

## Ageing procedure

The ageing procedure consists in exposing samples of the composite material in an aggressive environment that can be natural or artificial. In the frame of the project, 2 relevant natural and 1 artificial environment were chosen.

The natural environments are Tecnalia exposure sites that are referred as HarshLab and Port of Pasaia. The artificial environment is a cyclic ageing procedure combining various ageing process in specific equipment.

The natural degradation is usually a quite slow and complex process the main objective is designing an accelerated artificial ageing in laboratory that generate damage that are close enough to the one observed in natural sites. Ideally an acceleration factor can be calculated that may give a relationship between the time spent in accelerated ageing cycle and the potential lifetime in natural environment.

### Natural environment: HarshLab

The HarshLab [9] is a Tecnalia facilities that consists in a 4m diameter buoy installed in the bay of Biscay near the town of Armintza (Basques country, Spain) in the Biscay Marine Energy Platform (BiMEP) (see Figure 1).

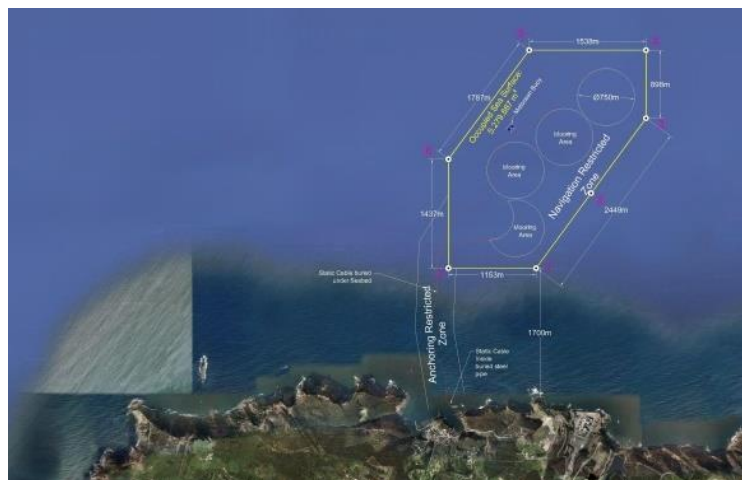


**Figure 1: Location of HarshLab in the BiMEP area**

The buoy is equipped with racks for samples exposition in 3 different areas: the atmospheric, the splash, and the immersed area (see Figure 2). The sea conditions and the atmospheric parameters are monitored in the BiMEP and the overall environment is typical of offshore condition with strong waves.



**Figure 2: aspect of the HarshLab before installation, view on the immersion area**

The NEMMO material samples were installed in the immersion zone with the help of specifically design racks, as it can be seen in the Figure 3.



**Figure 3: manipulation of the immersed racks to access to the immersed samples**

The samples were exposed for 10 months with 2 intermediate inspections.

#### Natural environment: Port of Pasaia

The second exposition site in natural environment is the Tecnalia exposition facility in the port of Pasaia. Pasaia is a town situated in the Basques country in Spain. The port is not directly open to the sea but connected with a channel (see Figure 4). The environmental condition (sea and atmosphere) are followed by the AEMET weather station situated in the channel access to the sea [10].

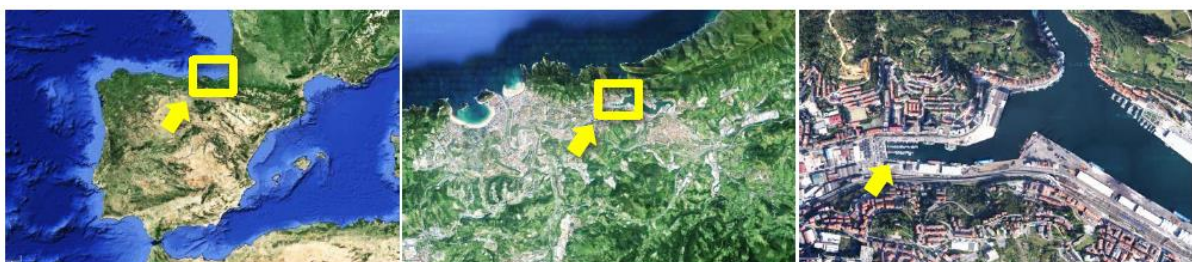


**Figure 4: location of the exposition facility in the port of Pasaia**

The environmental condition is not so representative to offshore condition and are closer to estuary condition. Nevertheless, the area is well known for a rapid biofouling growth[11], that makes it relevant to assess the material behaviour in presence of biofouling.

The NEMMO samples were installed in immersion fixed on racks that can be directly accessible from one of the piers of the port. They were exposed for 10 months with 2 intermediate inspections.

### Accelerated ageing in laboratory

In order to predict long-term behaviour of the composites, "accelerated aging" of the material is frequently performed.[12] As a 25-year lifetime requirement is commonly specified in the renewable marine energy industry, the accelerated test protocol must aim to reproduce the effects of 25 years exposure in a few months. Accelerated testing is also a valuable tool for rapid comparison of different material options[1].

There are at least three ways of accelerating tests; increasing test temperature is the most common but raising stress levels or reducing sample thickness can also enable a particular damaged state to be reached quicker[2].

In terms of water diffusion and chemical degradation, the accelerating factor generally retained is the temperature. The degradation processes are assumed to be thermally activated following an Arrhenius law as:

$$s = A \exp (-B/T) \quad (1)$$








with  $s$  = rate of the phenomena,  $A$  and  $B$  are constants, and  $T$  is the absolute temperature.[12] As a very rough guidelines a 10 degree increase in the temperature of a chemical reaction responsible for the degradation, accelerates approximately two times the reaction rate. The degradation kinetics however are more complexed and difficult to model.[13]

To most frequent aging procedure of FRC for tidal turbines is accelerated aging in seawater at elevated temperature (hydrothermal). Additional mechanical stress such as sustained bending or hydrostatic pressure can be applied to further approximate the real operating conditions[1], [14]. Monitoring the evolution of physicochemical parameters during the aging as well as comparing the materials characteristics in its initial state with those of the aged material sheds light on the relative resistivity of the material under operating conditions.

The NEMMO project seeks to generate the necessary models, knowledge, designs, and testing procedures to develop larger, more efficient, and more durable composite tidal turbine blades. As initially planned, a starting point for the accelerated aging protocol is the ISO 12944 (2018) part 9 Annex, which is a robust corrosion testing procedure for offshore and marine environments. This aging protocol needs to be adapted for the composite material and the specific application of the tidal blades.

Based on the scientific literature TECNALIA has designed an accelerated aging protocol for composite testing. The accelerated aging will be performed as cyclic aging based on the standard ISO 12944. The testing conditions need to be adapted for the purpose of the study. One cycle consists of seven days testing under the conditions indicated in Table 1.

**Table 1 An aging cycle**

	<i>Day 1</i>	<i>Day 2</i>	<i>Day 3</i>	<i>Day 4</i>	<i>Day 5</i>	<i>Day 6</i>	<i>Day 7</i>
							
<b>Aging media</b>	Condensation 24h	Condensation 24h	Immersion seawater 24h	Immersion seawater 24h	Immersion seawater 24h	Immersion seawater 24h	Immersion seawater 24h
<b>Temp.</b>	T=50°C	T=50°C	T=30 °C	T=30 °C	T=30 °C	T=30 °C	T=-2 °C
<b>Radiation</b>	12h UVA 340, 0,68 W/m <sup>2</sup> 12 h OFF	12h UVA 340, 0,68 W/m <sup>2</sup> 12 h OFF					

The aging conditions are as follows:

- **Days 1, 2:** 24 hours water condensation at 50°C combined with 12 hours periods of UV illumination. An irradiance level of 0.68 W/m<sup>2</sup> at 340 nm was chosen to match the typical maximum irradiance of summer sunlight at noon[15]. The UV/condensation chamber is presented in the Figure 5.



**Figure 5: Tecnia chamber for UV/condensation ageing**

- **Days 3-6:** Immersion in seawater at 30°C. The elevated temperature, selected to accelerate the degradation process, is low compared to the glass transition temperature of most polymeric matrices. Thus, it can be safely assumed that the degradation mechanisms themselves would not be affected[15]. The immersion was done in a specific tank designed by Tecnia and filled with a synthetic sea water prepared according to the recommendation of the standard ASTM D1142 [16]. There is a compensation tank to prevent any level lowering due to evaporation, a set of heating system for temperature control and a recirculation pump to provide a constant oxygenation and homogenization of the synthetic sea water as seen in the Figure 6.



**Figure 6: Tecnalia immersion tank for artificial ageing**

- **Day 7:** Immersion in seawater at  $-2^{\circ}\text{C}$ . The aim is to simulate low temperature conditions in sea, approaching the lowest possible temperature of the seawater without freezing. The ageing was performed in a small synthetic sea water (ASTM D1142 [16]) tank placed in a climatic chamber (see Figure 7) at  $-2^{\circ}\text{C}$ .



**Figure 7: Tecnalia climatic chamber used for the thermal shock ( $-2^{\circ}\text{C}$ )**

The full accelerated ageing test consists in performing **20 cycles**.

#### Ageing procedure summary

*The ageing will be performed in 2 natural sites: the HarshLab that is very representative of offshore conditions and the port of Pasaia for the high amount of biofouling growth.*

*A laboratory accelerated ageing test was defined and will consist of 20 cycles of: 2 days of UV/condensation, 4 days of immersion in synthetic sea water and a thermal shock in climatic chamber (1 day)*

## Characterization of the materials and the aging process

The second step of the study consists in defining which characterization methods are available and suitable to assess the damage that suffered the composite material during the ageing process.

The cited standards will serve as a guideline and they will not be strictly followed for all the methods.

For the “surface” characterization methods, such as differential scanning calorimetry (DSC) and infrared spectroscopy (FTIR), the gel coat was characterized as it is the material in contact with the sea water. To do so, the gelcoat was scraped and turned into powder (Figure 8).

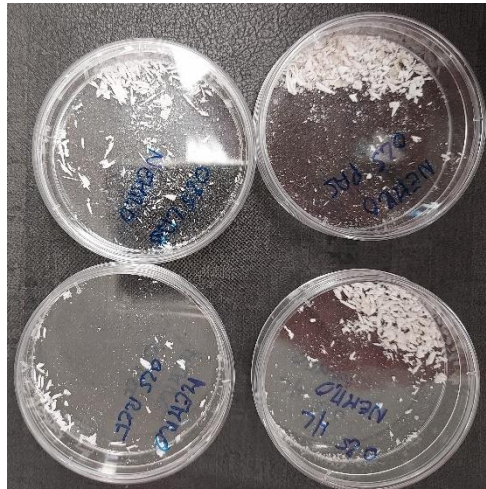


**Figure 8: scrapped power from the sample’s gelcoat for DSC analysis**

For the other methods (gravimetry, tensile test...) the whole sample (composite and gelcoat) was tested.

### Physicochemical methods:

#### Gravimetry

Controlling the weight gain during aging in seawater allows for the monitoring of the water absorption phenomenon. To do so, the sample is first weighed in its initial dry state and its initial mass ( $w_0$ ) is recorded. Then the immersed material is regularly weighed throughout the immersion period and the intermediate weight ( $w$ ). It is then possible to determine the water mass either as fraction or percentage and quantify the diffusion behaviour of water in a composite material by applying the equation:[17]

$$m = (w - w_0)/w_0 \times 100 \quad (2)$$

The suggested size of the specimen is 50x200mm. Alternatively square samples 100 x 100 mm can be used (Figure 9). The number of samples recommended by the standard is 5. The suggested numbers of sample to be studied is 3.

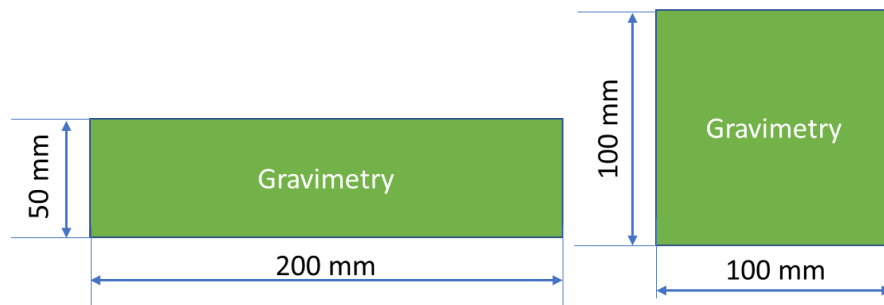


**Figure 9: Samples for gravimetrical analysis**

Gravimetry was performed on samples of 100\*100mm with the help of the precision scale presented on the Figure 10.



**Figure 10: precision scale for gravimetric measurement**

### **Differential Scanning Calorimetry (DSC) according to ISO 11357**

DSC is used to characterize the glass transition temperature of the composite. The glass transition temperature ( $T_g$ ) is useful to determine the maximum sea water ageing temperature for accelerated conditions. As sea water ageing can affect the material glass transition ( $T_g$ ), additional DSC measurements allow to follow the evolution of the  $T_g$  during the immersion of composites in sea water.

Samples weight should be in the range 5-100 mg. They are placed in tiny capsule containers and then in the DSC device (Figure 11).



**Figure 11: on the left: samples container in the sample holder of the DSC device (one is the reference and the other contains the gelcoat sample), on the right an overview of the DSC device used**

The DSC was performed from  $-90^{\circ}\text{C}$  to  $250^{\circ}\text{C}$  at  $20^{\circ}\text{C}/\text{min}$ .

#### **Thermal Gravimetric Analysis (TGA) according to ISO 11358**

TGA gives information about the thermal stability of the composite as well as the degradation mechanism (decomposition temperature, weight loss as a function of temperature, stepwise degradation process etc.).

Samples should be in the range 10-100 mg.

As there is no expected degradation due to thermal effect, TGA was not considered relevant for the material characterization.

#### **Fourier Transform Infrared Spectroscopy (FTIR) according to ASTM E1252 – 98**

FTIR spectra gives information about the chemical characteristics of the composites (polymerization and curing degree) as well as the degradation chemistry (degree of cross linking, scission reactions during aging). They will be cut from a bigger sample.

For recording the IR spectra, 1mg of the samples will be ground into powder with infrared-grade. KBr 100 mg will be used to prepare pellet (see Figure 12 and Figure 13).



**Figure 12: 1.2mm diameter KBr pellets with gelcoat powder for FTIR characterization**

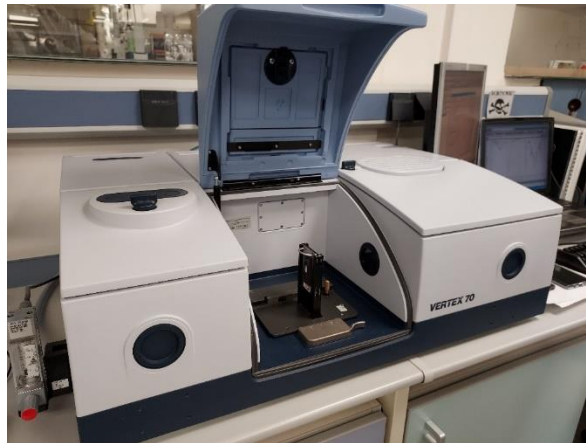


**Figure 13: FTIR device**

## Mechanical methods

### Tensile test according to ASTM D3039

This test method determines the in-plane tensile properties of polymer matrix composite materials reinforced by high-modulus fibres. A thin flat strip of material having a constant rectangular cross section is mounted in the grips of a mechanical testing machine and monotonically loaded in tension while recording the force. The ultimate strength of the material can be determined from the maximum force carried before failure. If the coupon strain is monitored with strain or displacement transducers then the stress-strain response of the material can be determined, from which the ultimate tensile strain, tensile modulus of elasticity, Poisson's ratio, and transition strain can be derived.[18]

The testing coupon with its dimensions is shown in Figure 14. Sample dimensions may vary upon fibre orientation. Tabs might be required. The number of samples envisaged by the standard is 5.

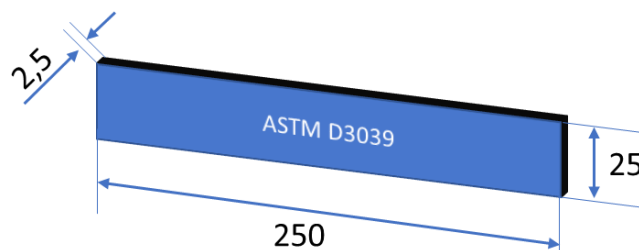


**Figure 14: Sample for tensile testing**

Tensile test was considered relevant for the characterization of the material ageing. Tensile tests were performed on INSTRON 5500R with a load cell of 100kN and 5585H with a load cell of 250kN and a clip-on extensometer.



**Figure 15: Instron 5500R (left), 5585H (right)**

### Shear test according to ASTM D5379

This test method covers the shear properties of composite materials reinforced by high-modulus fibres. A material coupon in the form of a rectangular flat strip with symmetrical centrally located v-notches is loaded in a mechanical testing machine. The specimen is inserted into the fixture with the notch located along the line of action of loading by means of an alignment tool that references the fixture. The two halves of the fixture are compressed by a testing machine while monitoring load. The relative displacement between the two fixture halves loads the notched specimen and the shear response of the material can be measured.[19]

The testing coupon with its dimensions is shown in. Sample dimensions, especially thickness, may vary upon fibre orientation. Tabs might be required. The number of samples envisaged by the standard is 5.

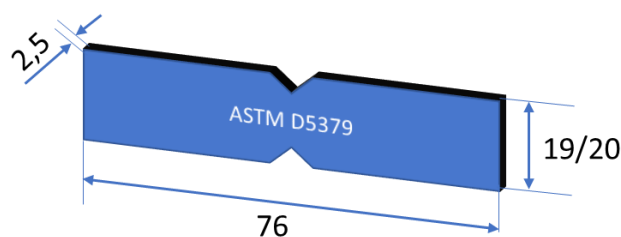


**Figure 16: Sample for shear test.**

Shear test was not considered relevant for the characterization of the ageing of the material. It is relevant in the frame of the NEMMO project but covered in the WP4, specifically in the tasks related to fatigue assessment.

### Flexion test according to ASTM D7264

This test method determines the flexural properties (including strength, stiffness, and load/deflection behaviour) of polymer matrix composite materials under the conditions defined.[20]

The sample dimensions are depicted in Figure 17. Dimensions may vary depending on testing equipment.

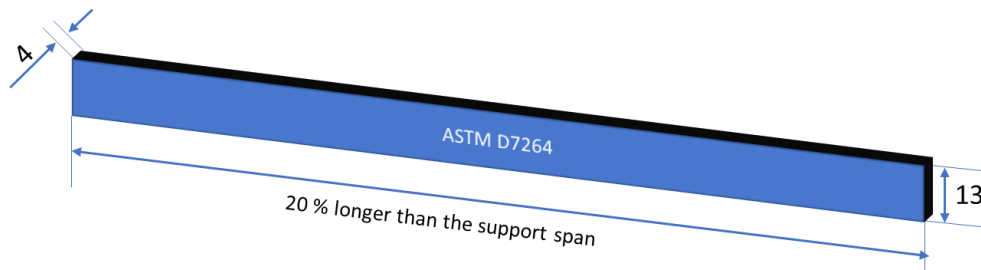


**Figure 17: Sample for flexion test**

Flexion test was not considered relevant for the characterization of the ageing of the material at this step of the project. Flexion test is usually reflecting the tendencies that are already observed with the tensile test.

#### Optical methods

Optical method such as photography and optical microscopy at low magnification were used to complete the degradation assessment study.

Digital camera was used to take pictures during the visual inspection in the natural exposition sites and all along the ageing and characterization process.

Optical microscopy with a low magnification binocular coupled with a digital camera was used to take pictures of material cross-section (Figure 18).



**Figure 18: binocular setup with image acquisition system**

#### Material characterization summary

*To characterize the damages suffered by the material during the ageing process, the following methods will be used: Optical assessment, gravimetry, fast Fourier transform infrared spectroscopy (FTIR), differential scanning calorimetry (DSC) and tensile test.*

## Experimental campaigns

The experimental campaign started with the reception of the material and the preparation of the samples. Then the ageing was performed as presented earlier in the document.

### Material

The material consisted in a large glass fibre reinforced vinyl ester panel covered with a white unsaturated polyester gelcoat. The material was fabricated and provided by CANOE.

It was then machine in 4 different sets of samples:

- One for initial characterization
- A second for the accelerated ageing test in the Tecnia's laboratories
- A third was put in immersion in the HarshLab exposition facility
- A fourth was put in immersion in the port of Pasaia exposition facility.

For each set, the amount, size, and shape of samples correspond to the requirement of the characterization tests that were mentioned earlier. The Figure 19 shows some of the samples that were prepared for ageing.



**Figure 19: example of the aspect of the sample after machining: on the left: gravimetric sample for the HarshLab, on the right: panel to extract sample for tensile test after aging**

To avoid unrealistic behaviour, the side of the sample were cover with mastic paste (Sikaflex) to prevent water uptake from the cutting edge (see Figure 20: sample with cutting edge protection).

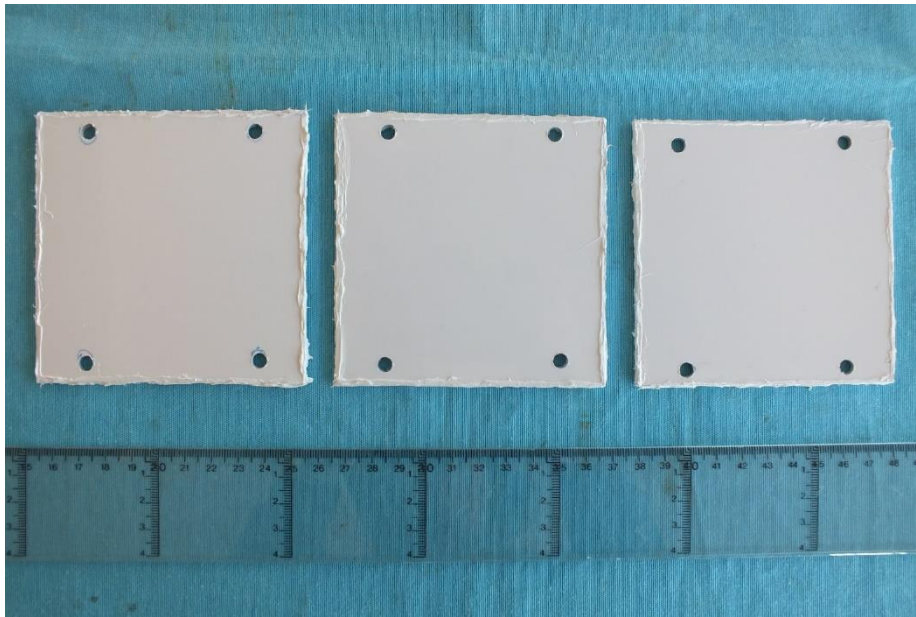


**Figure 20: sample with cutting edge protection**

**HarshLab: ageing and experimental issues**

The samples were immersed in the HarshLab facility in February 2020 (see Figure 21)



**Figure 21: samples fixed on the rack before immersion, HarshLab, February 2020**

The first visual inspection took place on May 2020 after 3 months of ageing. The aspect of the samples is reported on the Figure 22. After only 3 months, there is already a large amount of fouling that grew at the surface of the samples, including: shell (mussels), algae, worms and crabs and barnacles. The bio fouling is already completely occluding the surface from UV radiation. **Due to a tempest episode some of the samples were lost between the installation and the first inspection.**

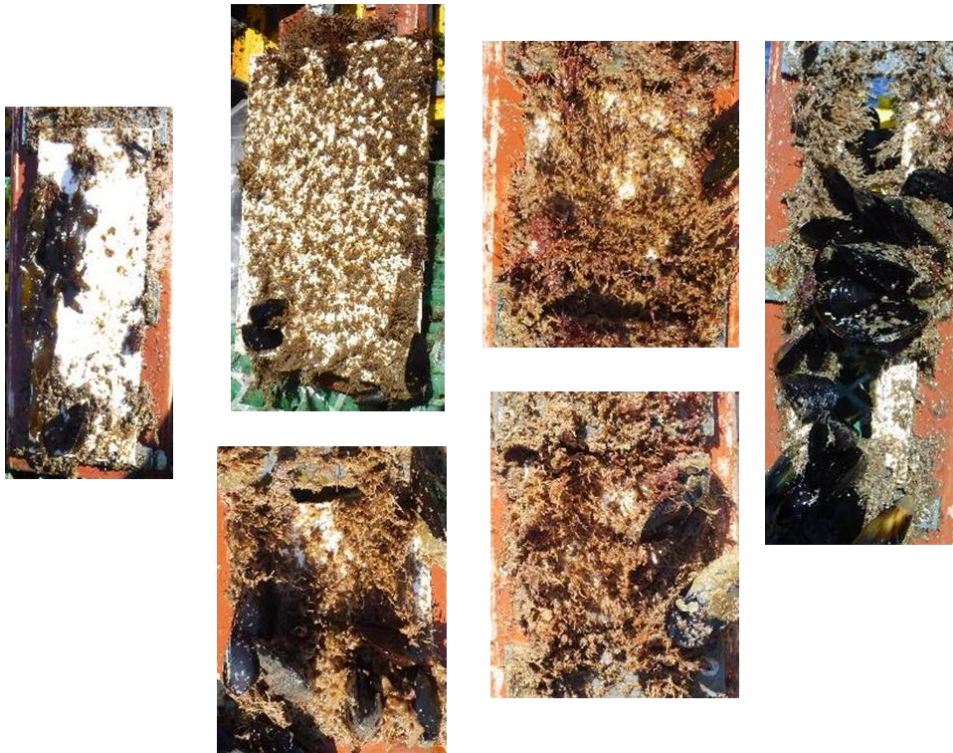


**Figure 22: aspect of the samples immersed on the HarshLab facility after 3 months of ageing**

The second inspection took place in September 2020 after 7 months of ageing.

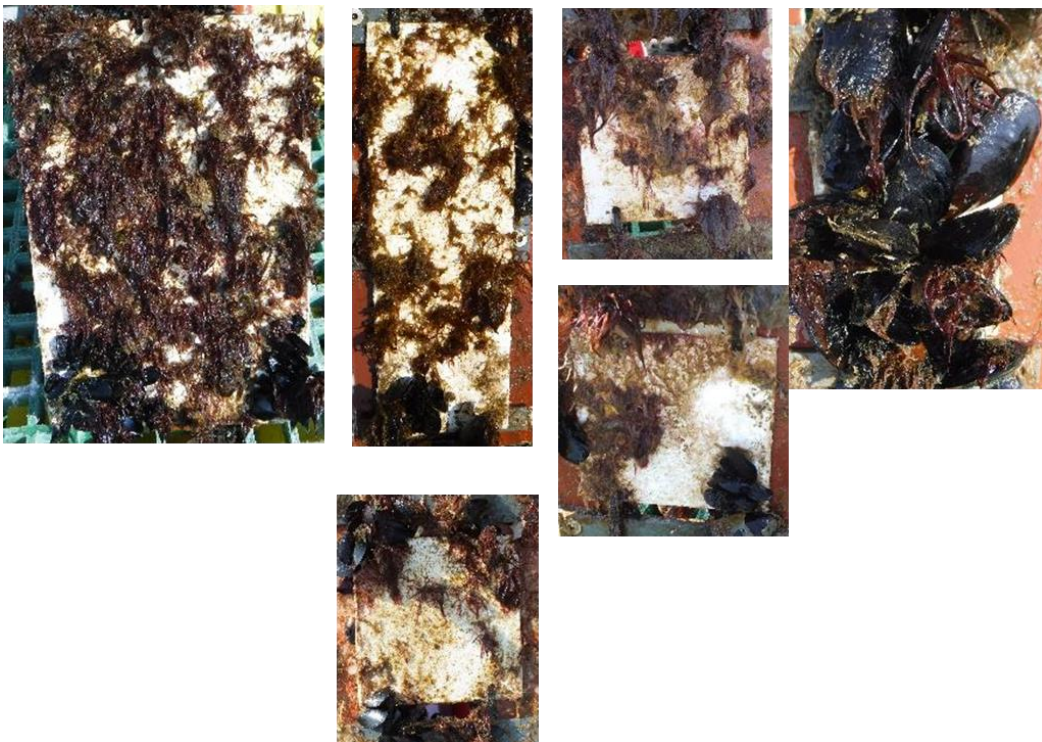


**Figure 23: aspect of the samples immersed on the HarshLab facility after 7 months of ageing**

The Figure 23 reports the aspect of the samples. The biofouling slightly diminished as the summer period was ending but remained quite important.

The samples were removed in December 2020 after 10 months of immersion (Figure 24). The biofouling was then clean and removed from the surface. This cleaning step was particularly challenging as some of the organisms such as barnacle were extremely well attached to the material. A high-pressure water jet cleaning was sufficient to remove most of the fouling such as the mussels or algae, but the barnacle shells had to be removed mechanically with a scrapping tool. Even with such tools, the base of the barnacle shell could not be completely removed (Figure 25).



**Figure 24: HarshLab Samples after 10 months of immersion before fouling cleaning**



**Figure 25: HarshLab Samples after 10 months of immersion after fouling cleaning**

### Pasaia Port

The samples were immersed in the port of Pasaia on February 2020. Figure 26 shows the samples installed on the racks before immersion.



**Figure 26: samples fixed on the rack before immersion, Pasaia port, February 2020**

The first inspection took place 3 months later in May 2020. By this time, a biofilm mixed with organic material started to cover the surfaces of the samples. Some microorganisms were also present such as larvae, water worms...as it can be seen on the Figure 27



**Figure 27: aspect of the samples immersed on the Pasaia port facility after 3 months of ageing**

Samples were then inspected at month 8 in October 2020. At this time, most of the samples surfaces was cover with small barnacle as shown in the Figure 28



**Figure 28: aspect of the samples immersed on the Pasaia port facility after 8 months of ageing**

The samples were removed from the exposition site after 10 months of ageing. The Figure 32 presenting the aspect of the samples before cleaning shows that the barnacles grew during the last months of immersion for a complete coverage of the samples.

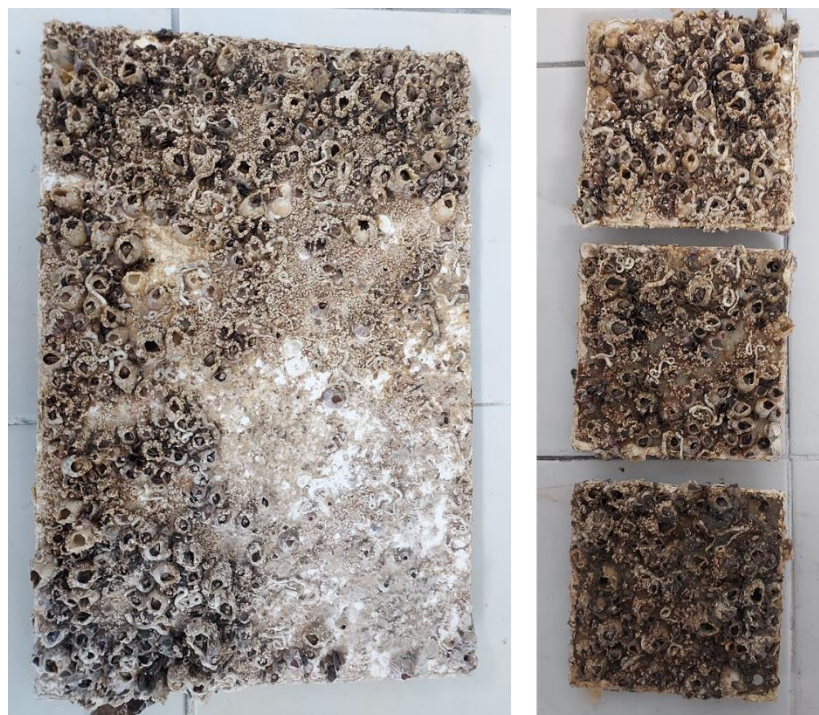


**Figure 29: samples after 10 months of immersions in the port of Pasaia before cleaning**

The section presented in the Figure 30 gives a good overview of the biofouling thickness that developed during the ageing period in the port pf Pasaia. As most of this biofouling was barnacles, the cleaning challenge was even higher than for the samples coming from the HarshLab. The same method of high-pressure water jet followed by mechanical scraping was used with a limited success as it can be seen on the Figure 31.



**Figure 30: section of a sample exposed in the port of Pasaia for 10 months.**



**Figure 31: Aspect of the samples immersed in the port of Pasaia after cleaning**

### Accelerated ageing test: ageing and experimental issues

The accelerated ageing cycle was performed from November 2020 to April 2021. The artificial ageing was delayed compared to the natural ageing because of the organizational issues coming from the restriction due to the COVID pandemic and the availability of the ageing chambers.

No visual change of the samples could be observed during the artificial ageing as shown in the Figure 32.



**Figure 32: Aspect of the sample during the accelerated ageing test**

Towards the very end of the ageing cycle, the panel dedicated to the mechanical tensile test was accidentally broken during the operation of moving the sample from the immersion tank to the climatic chamber.

To limit the loss of information, a quick ageing consisting only of a 2 months immersion was performed on a new panel to perform mechanical tensile test. The first reason to perform such “limited ageing” came from other information that are presented later in this report showing that UV exposition has a neglectable effect. Moreover, time was lacking to perform a completely new ageing. Finally, it was decided to add a reference material set in the WP4 testing campaign to check the reproducibility of the results presented here and fulfil the gap of data.

### Summary of the experimental campaign

*The experimental campaign was challenging with some issues related to the loss or the destruction of samples and restriction due to the COVID pandemic that lead to data gap (that will be filled in the next WP4 experimental campaign) and delay.*

*Both natural exposition site shows a strong growth of the biofouling that cannot be reproduce in laboratory. At this point, it will be extremely hard to be able to calculate an acceleration rate between natural and accelerated ageing.*

## Damage assessment and discussion

The material was characterized before and after aging. Intermediate characterization during the aging were done in the case of gravimetric measurement for accelerated ageing samples.

### Characterization

As mentioned before, FTIR and DSC were performed on the gel coat as it is the barrier between the composite and the water while gravimetry and tensile test were done on full system samples (composite and gel coat).

### Visual

Beside the general aspect of the samples and seeing the strong adherence of the barnacles on the gel coat, it is important to observe how is the interface between the shell and the gel coat. The aim is to see if the barnacle produced damages, mainly cracks or preferential pass for water penetration in the gel coat. Cross section was done in area where barnacles were stuck to the material. The Figure 33 present such interface. It can be clearly seen that the barnacle does not affect the integrity of the gel coat.



**Figure 33: cross section of a sample immersed in the port of Pasaia showing the interface between barnacles and gel coat**

### Gravimetry

Gravimetric measurements were done before and after ageing for all the ageing types (natural and artificial). In the case of the artificial ageing, extra gravimetric measurements were done each month during the ageing process.

For each gravimetric point, 5 weight measurements were done on three different samples. The statistical processing of the data was done in the software Statgraphics 18 to extract the average weight for an ageing type and ageing time associated with an error bar corresponding to a 95% confidence interval. The Figure 37 shows a summary of all the measurements done.

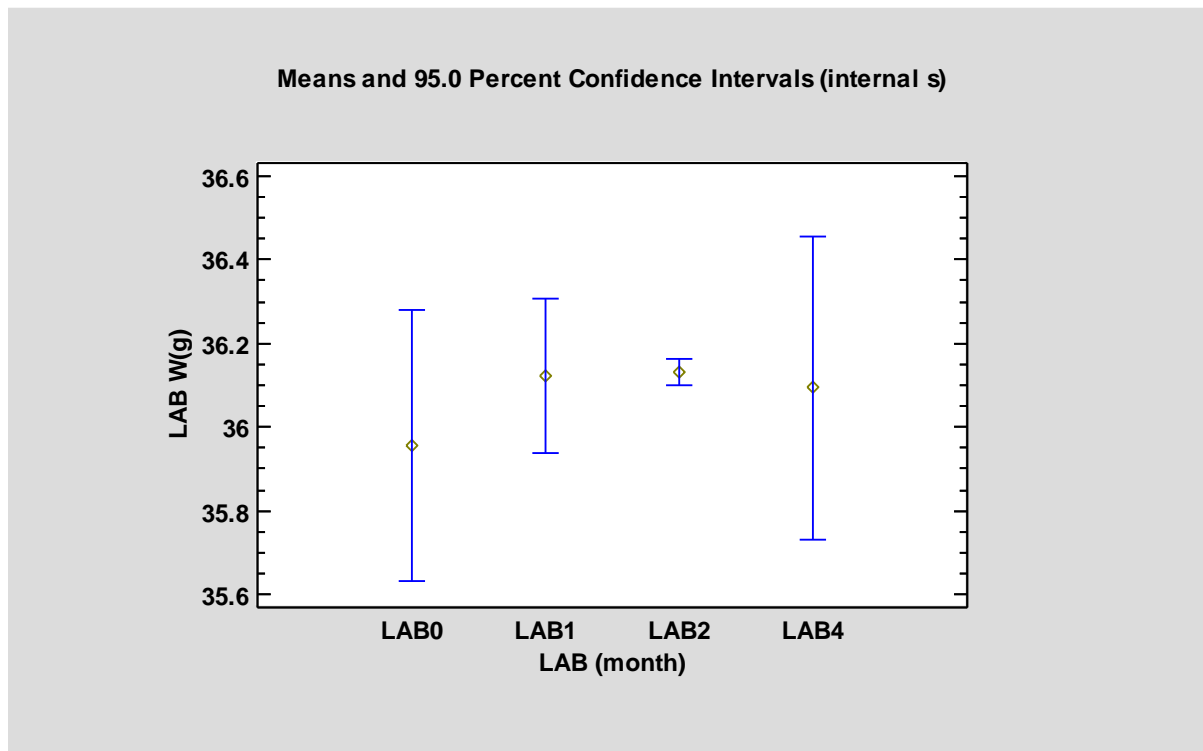


**Figure 34: gravimetric measurements on samples taken very month from the accelerated ageing test**

The Figure 34 presents the results obtained during the accelerated ageing. In this case, there is no biofouling effect so positive weight evolution would be only linked with water uptake. The relatively large error bar for a weight measurement comes from the fact that the sample are “wet”, and the surface drying is not always the same from one measurement to another. All the confidence interval overlapped so, from a strict statistical point of view, the right interpretation would be that there is no difference between the 4 points. Nevertheless, a less conservative interpretation concludes that there is a difference between the initial time (LAB0) and the other measurements indicating that water is penetrating in the material during the first month of immersion and reach saturation, so the weight does not evolve anymore during the rest of the immersion time. The water abortion at saturation is in average 0.45% of the mass of the sample.

The gravimetric measurement obtained on samples aged in the HarshLab are plotted in the Figure 35. With the strict statistical interpretation, there is no difference between the measurements. Mainly there is an outlier measurement in the HLO measurement that enlarge the confidence interval, the source of the error could not be identified. The large interval on the HL10 measurement comes from the variable amount of barnacle shell remaining at the surface of the samples.

The Figure 36 presents the results obtained on the samples aged in the port of Pasaia. A very clear difference of mass can be seen between and after ageing. That correspond to a 3.17% mass increase that is much higher that the effect of the water uptake (0.45%). This difference can be easily explained by the presence of barnacle shell remaining that cover almost homogenously the surface of all the samples.

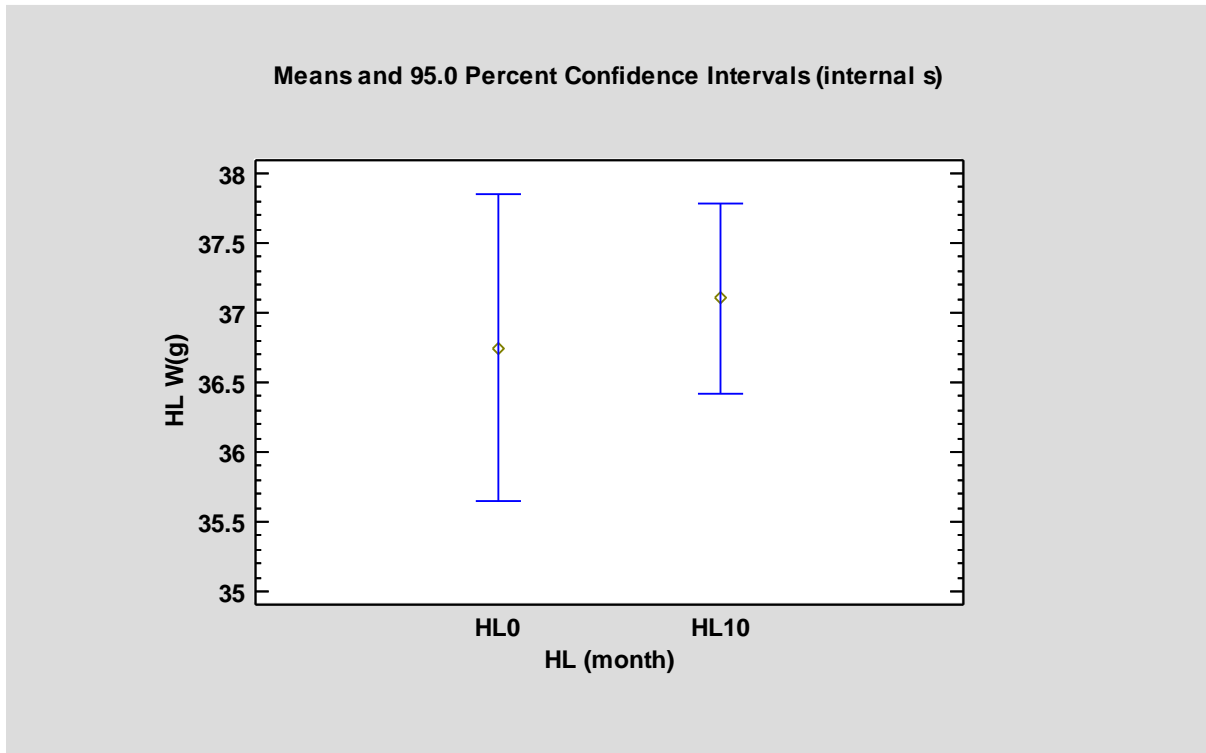


**Figure 35: gravimetric measurements done before and after ageing in the HarshLab facility**

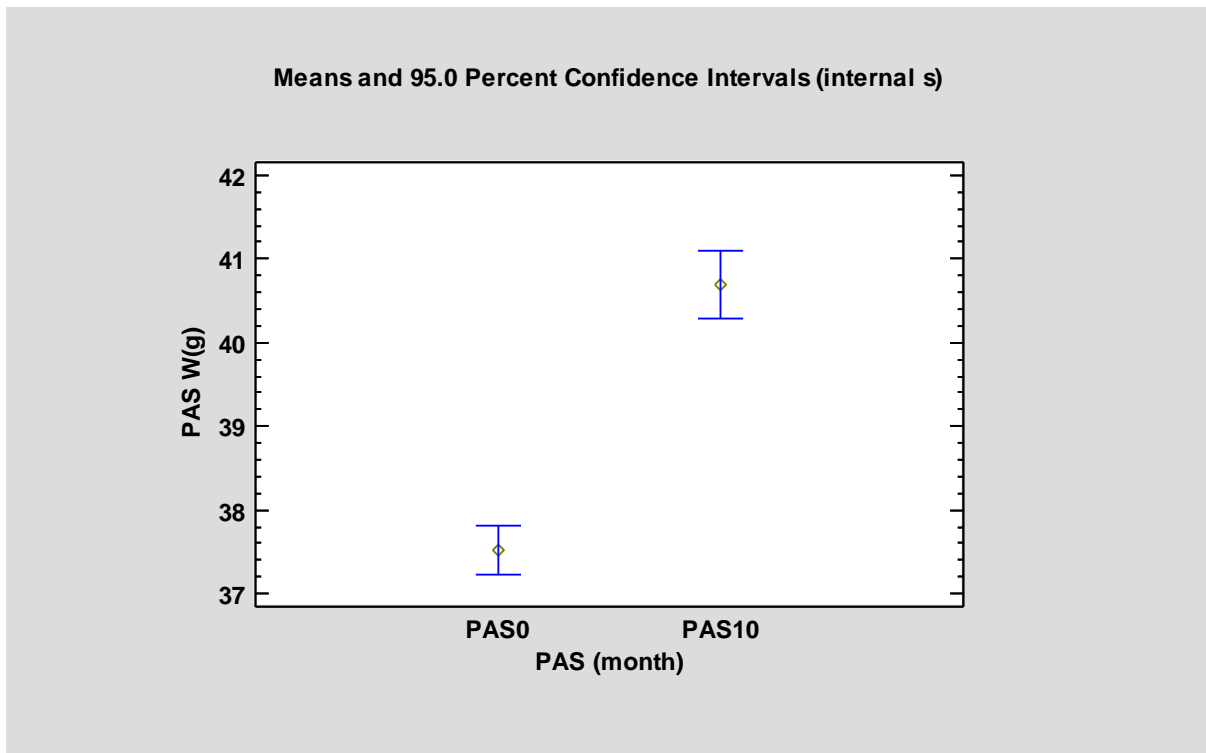


**Figure 36: gravimetric measurements done before and after ageing in the port of Pasaia**

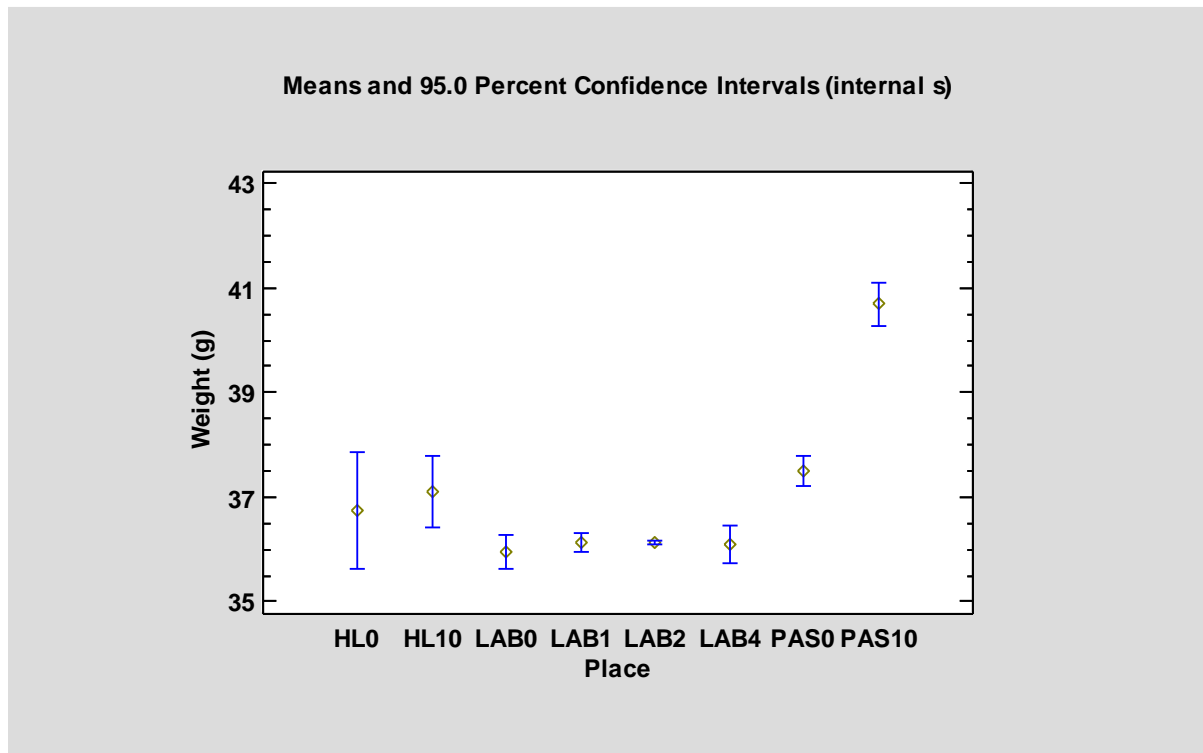


**Figure 37: summary of all the gravimetric measurement done**

To summarize, the water uptake can be only assessed for the accelerated ageing test and correspond to 0.45% of the sample mass. For both natural ageing, the gravimetric test was completely dominated by the biofouling remaining that it could not be eliminated without damaging the samples.

### Fast Fourier infrared spectroscopy (FTIR)

The Figure 38 presents the FTIR spectra that were obtained on the gelcoat before ageing (NEMMO 025 Ref), after the accelerated ageing process (NEMMO 025 LAB), the ageing in the port of Pasaia (NEMMO 025 PAS) and the ageing in the HarshLab (NEMMO 025 HL). The aim is to assess the chemical stability of the gel coat material that is the barrier between the composite, a priori more sensitive to the water penetration, and the sea water.

All the spectra obtained are similar, with a large peak around  $3500\text{cm}^{-1}$  usually associated with the O-H (hydroxyl) group, a thinner peak around  $2800\text{cm}^{-1}$  that can be associate to  $\text{CH}_x$  groups and a thin and intense peak around  $1700\text{cm}^{-1}$  that can be attributed to the C=O (carboxyl) group that is part to an ether functional group. The region between  $1500$  and  $500\text{cm}^{-1}$  also known as the fingerprint is quite complex to interpret with a dense peak forest. The comparison between the spectra obtained and the spectra database of the FTIR software suggest that the closest spectra from our measurement is a polyester unsaturated isophthalate (reported in purple on the Figure 38) that makes perfectly sense for a gel coat.

The interesting point here is that there is no creation neither disappearance of peaks in our measured spectra indicated that whatever is the ageing, there no effect on the chemical structure of the gel coat. Any modification of the chemical structure could come from a hydrolysis or a photooxidation. In the case of the natural ageing, the biofouling completely covers the sample, blocking the UV radiation.

Nevertheless, no modification was observed during the accelerated ageing test, with no biofouling, suggesting that the material is stable with the time.

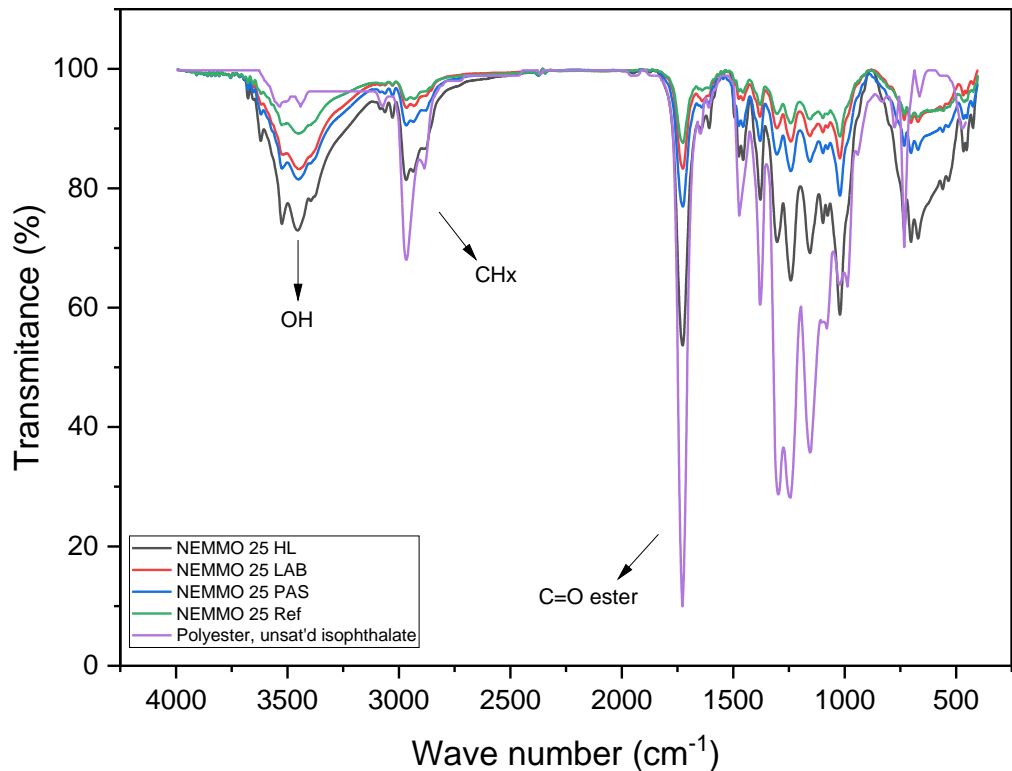


**Figure 38: FTIR spectra performed on the gel coat**

### Differential scanning calorimetry

DSC was performed on gelcoat samples before and after ageing. The DSC curve obtained on the gelcoat before ageing is presented on the Figure 39 as example. The aspect of the curve is not what was expected and lead to interpretation issues. The  $T_g$  cannot be clearly identify and the baseline was somehow of bad quality.

The bad quality of the measurement is attributed to the sample preparation. Indeed, the gelcoat was scrapped and reduce in powder in a mortar but it was challenging to obtain a homogeneous particle size, leading to inhomogeneous heating during the temperature ramp up.

Except if a more reliable sample preparation is set up or found, the DSC method cannot be use for material damage assessment.

Sample: NEMO 025 Ref  
 Size: 4.5000 mg  
 Method: Postcurados resina

DSC

File: C:\... \2021\ENERGIA\JB\NEMO 025 Ref.001

Instrument: DSC Q100 V9.9 Build 303

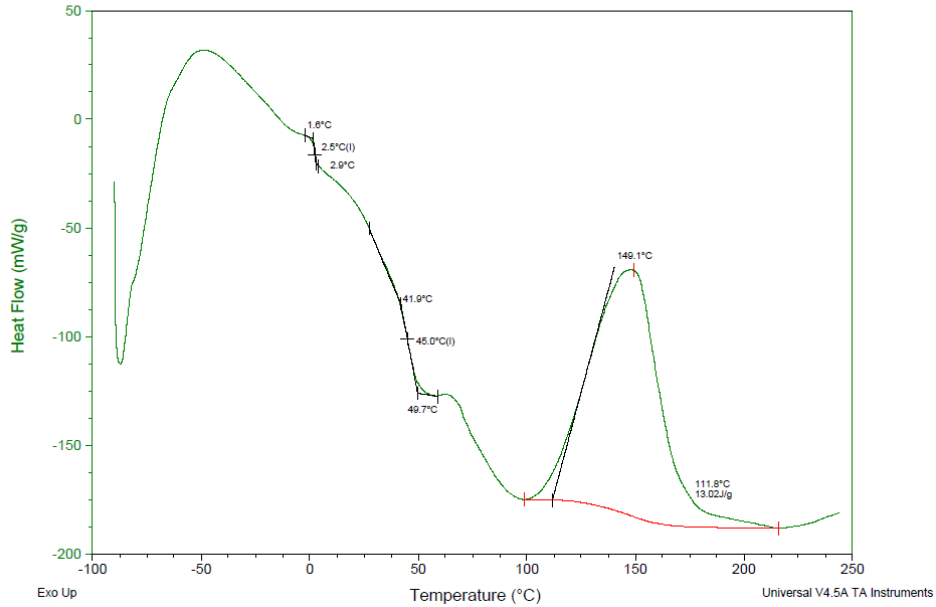


**Figure 39: DSC curve obtained on the gelcoat before ageing**

### Tensile test

The tensile tests were performed at a strain rate of 2mm/min with an extenso meter in order to calculate the modulus (see Figure 40). 5 samples taken from the panel at reception (without ageing) were tested and referenced as REF, 5 samples were extracted respectively from panel that was aged in the HarshLab (referenced as HL), in the port of Pasaia (referenced as PAS) and after the accelerated ageing test (referenced as LAB).



**Figure 40: sample during the tensile test**

Due to the way that the samples panels were cut before ageing, the fibres were oriented at 45° from the main stress direction. The consequence is that the modulus obtain is not representative of the real mechanical properties of the composite but is sufficient to compare the different ageing and their effect on the material properties.

From all these samples, one from the Pasaia gave an uninterpretable result that was discarded. The results obtained are presented in the Table 2.

**Table 2: Statistical summary of the modulus extracted from the tensile test.**

Place	Count	Average	Standard deviation	Coeff. of variation	Minimum	Maximum
REF	5	11.34	0.391152	3.44931%	10.9	11.8
HL	5	12.48	0.349285	2.79876%	12.1	12.9
LAB	5	11.16	0.0894427	0.801458%	11.1	11.3
PAS	4	11.75	0.404145	3.43953%	11.4	12.3
Total	19	11.6789	0.61335	5.25176%	10.9	12.9

The Figure 41 presents the average values of the modulus extracted from the tensile curves according to the ageing type. The error bars indicate the confidence interval at 95%.

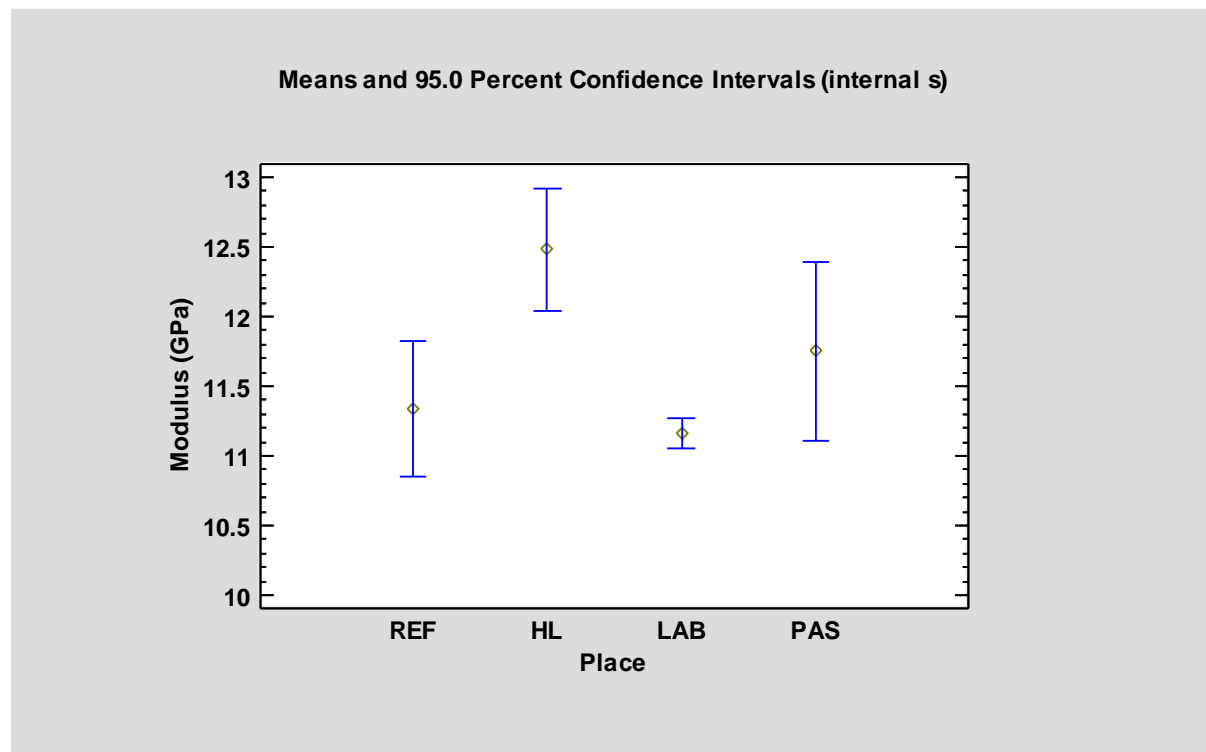


**Figure 41: Modulus extracted from the tensile curve according to the ageing type**

This figure indicates that the modulus does not change significantly according to the ageing (all confidence interval overlap). That indicates that the little amount of water that penetrates does not

foment a plasticization of the material leading to a diminution of the mechanical properties. Moreover, it also shows that the presence of the adherent biofouling does not affect the mechanical properties of the material.

### Discussion and recommendation for a novel test procedure

The damage assessment shows that beside a slight water uptake that was expected, there was almost no damage created in the material system (composite and gelcoat) during the ageing process, whatever if it was natural or artificial.

No effect of UV action could be identified, and it is not clear if the thermal lead to any ageing as the mechanical test would have been the characterisation test the most sensitive. For reminding, the artificial ageing panel for mechanical test was accidentally destroyed before the mechanical test could be done.

Mechanical tests indicate that the water uptake did not affect the mechanical properties during the ageing process.








The choice of the fibre glass reinforced vinyl ester composite coated with an unsaturated polyester gelcoat appears to be very reliable to be in operation in immersed sea water.

Overall, it seems that the main issue for the material system is the ability of the biofouling to grow quickly at the surface of the material with a very good adherence, mainly for the barnacle family of organisms.

The apparent absence of UV effect on the material ageing led to the decision to consider only the immersion test to perform the “emergency” ageing for a new panel after the accidental destruction of one of the panels during the accelerated ageing test.

For the next experimental campaign that will take place in the frame of the WP4, it is recommended to remove the UV exposition of the artificial ageing cycle and to keep the thermal shock.

The new cycle would be the following:

	Day 1	Day 2	Day 3	Day 4	Day 5	Day 6	Day 7
							
<b>Aging media</b>	Immersion seawater 24h	Immersion seawater 24h	Immersion seawater 24h	Immersion seawater 24h	Immersion seawater 24h	Immersion seawater 24h	Immersion seawater 24h
<b>Temp.</b>	T=30 °C	T=30 °C	T=30 °C	T=30 °C	T=30 °C	T=30 °C	T=-2 °C

### Summary of the damage assessment and discussion

*The characterization and the comparison of the properties measured before and after the ageing process did not show the generation of clear damages. There was a good agreement between the observation done after the natural and the artificial ageing.*

*Obviously, as no clear damage was identified and thus quantify, the acceleration factor could not be defined and calculated.*

*The choice of the fibre glass reinforced vinyl ester composite coated with an unsaturated polyester gelcoat appears to be very reliable for assets immersed sea water*

## Conclusion

During this task 2.4.1, an artificial ageing procedure was defined based on literature data and associated with a material characterization procedure for the reference material of the NEMMO project that consists in a glass fibre reinforced vinyl ester coated with an unsaturated polyester gelcoat.

3 different ageing were performed on panels made of this reference material. 2 of these ageing took place in natural environment. One was done at the offshore facility HarshLab where the panels were put in the immersion zone. The second ageing consisted in immersing the panels in the port of Pasaia expecting a high amount of biofouling. The third ageing was an accelerated ageing process following the artificial ageing mentioned earlier.

The results obtained showed that the material did not suffer from the ageing condition (both in natural and artificial ageing) indicated that it is a good choice for assets that operate in sea water.

Nevertheless, a high amount of biofouling grew at the surface of the sample during the natural ageing process (both in HarshLab and in the port of Pasaia), that may significantly affect the function of a tidal blade if it remained static.

With the acquired experience, a new ageing cycle was proposed for the accelerated ageing test.

That makes very promising the next experimental campaign that will takes place in the frame of the WP4 where new materials for tidal blade developed in the NEMMO project will be tested and in particular, antifouling coatings applied on top of the gelcoat.

## Task 2.4.2 Development of fouling test for tidal turbines composite blades in dynamic conditions in sea environments

### Overview of test conditions and design approach

Flow induced stresses have recently been shown to have a major impact on biofilm formation slowing down growth and reducing its sensitivity to surface properties [21]. Surface textures can be altered to enhance this effect by focussing stresses over exposed surfaces and minimizing surfaces available for secure attachment. A range of biomimetic textures have been investigated in Work Package 3 to identify the most promising and practical texture. The aim of the test procedures described in this section is to characterise biofouling formation and growth on four separate surfaces. Test surfaces will include the reference coupon made from the original blade composite material, the best performing biomimetic micro-texture and best performing coats incorporating novel multi-material solutions. The flat coupons will be immersed in sea water continuously over a period of 3 months and exposed to hydrodynamic stresses mimicking conditions expected over parts of the full scale NEMMO turbine.

A new and novel test platform is being designed at DCU to allow for a non-uniform stress distribution over sample surfaces. It will rely on a symmetrical 2 blade turbine rotating in the horizontal plane rather than the traditional cylindrical layout. The turbine blade radius will be  $R = 0.6m$ . The two blades will accommodate four flat coupons, one on each blade surface. Their dimensions are  $12\text{ cm} \times 34\text{ cm}$  starting at a radial position  $r = 21\text{ cm}$  along the blade centreline. The flow velocity over the test surfaces will more than double from the root to tip so that stresses will increase by more than 4. This ability to apply increasing stresses without changing the rotational speed provides for a closer comparison with hydro-turbine operation and is the key difference compared to traditional test platforms. The symmetrical arrangement will also expose the 4 test coupons to similar stress levels and will facilitate comparison between anti-fouling solutions. The design has relied on high fidelity Computational Fluid Dynamics simulations to estimate the stress distribution. These results have confirmed that correlations for flat plate do provide a good approximation of the wall stress and boundary layer growth provided that the curve flow path is taken into account (see Figure 42). Both factors influence the turbulent structures of flow interacting with the biofilm. It showed that the tidal flow expected at the deployment site will induce limited asymmetry in the stress distribution within one rotation between the advancing and receding blades. These CFD simulations have also been used to determine the blade profile and operating conditions which will limit cavitation and separation at the leading edge and blade tip.

The operating conditions have been selected to achieve dynamic similarity over part of the full-scale turbine at blade section *S9* assuming a tidal stream speed of  $2.5\text{ m/s}$  and a rotor speed of  $16.83\text{ RPM}$ . The stresses reproduced over the central part of the blade that is away from the local acceleration experience near the leading and trailing edges will cover conditions expected over the full pressure side of the full-scale turbine and 50% of the suction side on the downstream half of the blade surface.

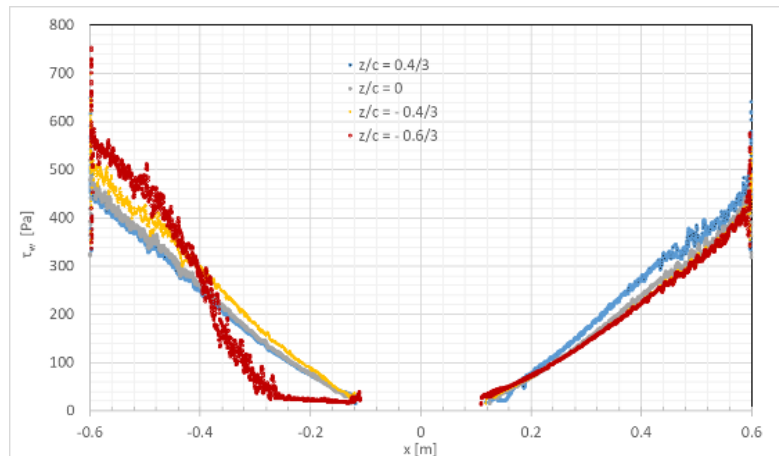


**Figure 42. Shear stress distributions along sampling lines aligned with the leading edge for both the advancing ( $x < 0$ ) and receding ( $x > 0$ ) blades relative to the incident tidal stream.  $z/c = 0.6/3$  refers to the sampling line at the edge of the test plate while  $z/c = 0$  is the central sampling line.**

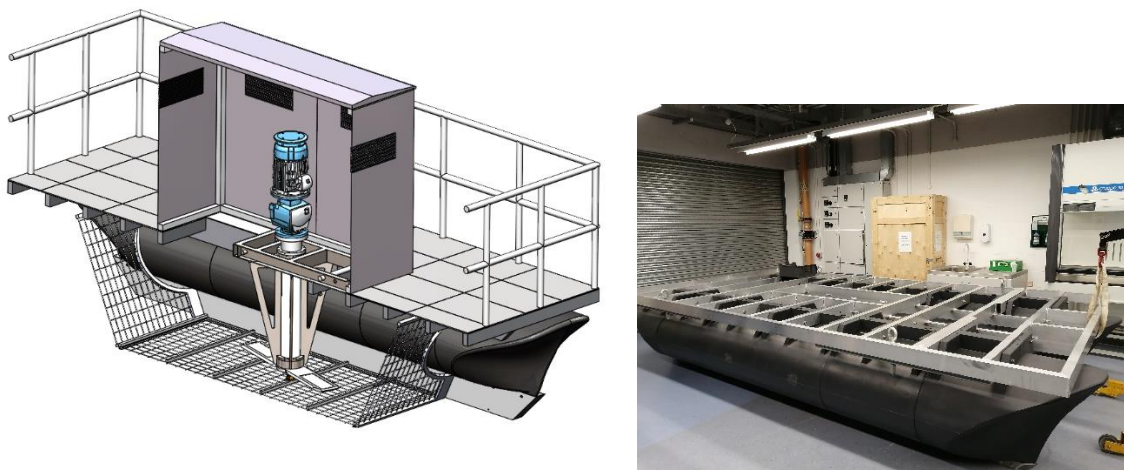


**Figure 43 Sea platform. [Left] CAD design incorporating the motor and turbine. [Right] Floating structure.**

## Detailed review of design

### Methodology

Computational Fluid Dynamics simulations were performed to test alternative turbine designs of the turbine profile and rotational speed. This was assessed in terms of the ability to

- reproduce turbulent conditions similar to those expected on the full-scale turbine,
- avoid cavitation at the blade tip, and
- minimize hydrodynamic torque on the full turbine.

Key features common to the successive design iterations include:

- blade cross section profile has constant chord length  $c = 0.3m$  over section starting at  $x/c = 2/3$  and extending to  $x/c = 0.565/3$

- The upper and lower surfaces are planar, and parallel to the plane of rotation to induce a flow similar to parallel flow over flat surfaces.
- The blade tips are curved with a constant radial coordinate  $r/c = 2$ .

The final design is based on curved leading and trailing edge to limit low static pressure zone due to flow acceleration. See Figure 44 for an outline.



**Figure 44 Design blade profile. [Left]: symmetrical profile and [Right]: Planar design at trailing and leading edges over upper surfaces.**

The turbine will operate at a rotation speed  $\omega_r = 30 \text{ rad/s}$  inducing a relative flow velocity of magnitude  $V_o = \omega_r r = 16.95 \text{ m/s}$  at  $r = 0.565$  that is at the edge of the blade section where the chord length is constant. This matched, by design, the relative maximum velocity expected over the Nemmo turbine over the blade section at radial position  $r = 9.5 \text{ m/s}$  under nominal conditions (tidal current at  $2.5 \text{ m/s}$  and turbine rotational speed  $16.83 \text{ RPM}$ ). It should be noted that the reduced chord length translates in a lower Reynolds number than expected on the full scale Nemmo turbine. Further analysis will be discussed in this report. The turbine is tested here in a tidal current of  $0.5 \text{ m/s}$ , that is approximately  $1 \text{ knot}$ .

The two equation  $k-\omega$  SST model of ANSYS Fluent version 2019 [22] with intermittency modelling was used for transitional turbulence modelling. All discretization schemes were second order in space and first order in time. A transient solution was performed. All data presented refers to instantaneous results at  $t_{su}/T = 5$  that is five blade revolutions.

A sliding mesh approach was used to account for the blade rotation with two concentric cylindrical zones. The inner zone rotates with the blade while the outer zone is stationary and fixed to the absolute reference frame. This approach makes it possible to account for the effects of a tidal current by specifying a fixed inlet boundary attached to the outer stationary domain. The vertical extend of the domain is  $L_z = 1.025 \text{ m}$ . The radius of the stationary and rotating domains relative to the turbine radius  $R_t$ , are  $R_s/R_t = 5$  and  $R_r/R_t = 1.5$  respectively. See Figure 45 for an outline description of the domain.

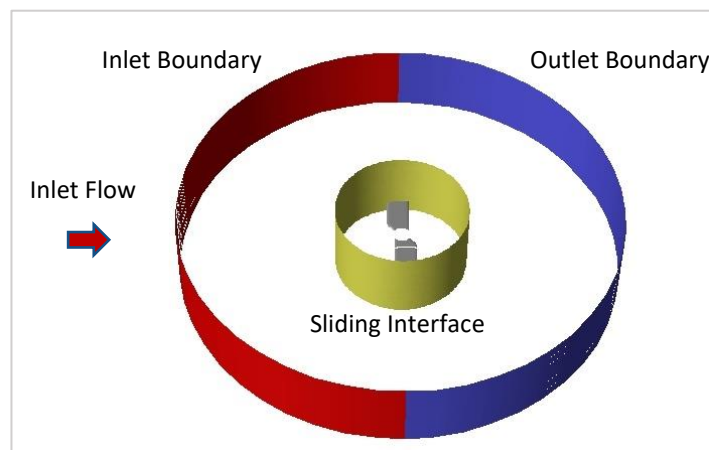


**Figure 45 Overview of computational domain**

The inner rotating zone was meshed with tetrahedral cells while a hexahedral cell is used in the outer fixed zone. Most results reported are based on Mesh M1 made of approximately  $40.5 \times 10^6$  cells. Meshing includes 25 prism layers attached to the blade surfaces meshed with  $\Delta_b = 1mm$  size face elements and a first layer cell height  $\Delta y_w = 12.5 \mu m$ . The target cell size in the outer stationary and inner rotating domains are  $\Delta_o = 0.4 m$  and  $\Delta_i = 0.03m$  respectively. A coarser mesh (M2) of approximately  $11 \times 10^6$  cell with  $\Delta_b = 2mm$ ,  $\Delta y_w = 25 \mu m$  with other parameters unchanged was also tested primarily to assess the sensitivity of wall modelling to the wall  $y^+$  resolution.

### Simulation results

The mesh M2 produced a wall  $y^+$  over the blade surface well in excess of 1 but below 12 (See Figure 46). Although a  $y^+ \sim 5$  can be expected to reproduce reasonable trends for wall shear stress over flat plate parallel flow, with accurate prediction at  $Re_x \sim 10^6$ , simulations can be expected to significantly under-predict by approximately 40% the skin friction with  $y^+ \sim 10$  [23]. By comparison the under-prediction is of the order of 6%  $y^+ \sim 5$ . The wall layer thickness was halved with the mesh M1 reducing the maximum  $y^+$  to  $y^+ \sim 6$ .

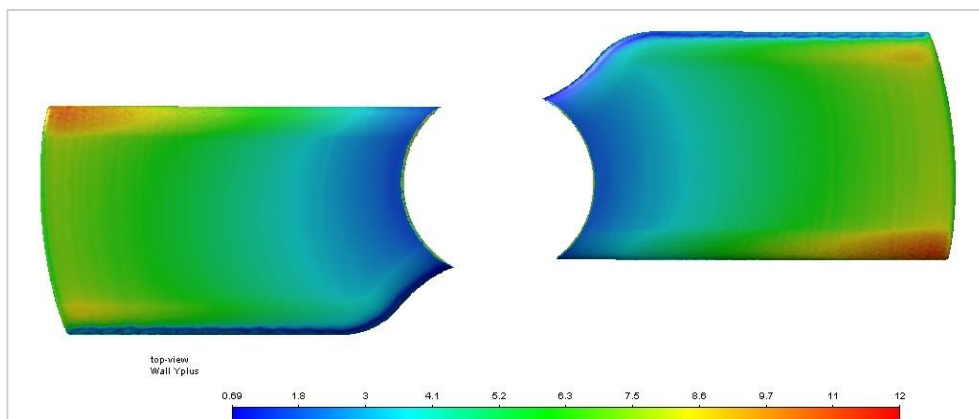


**Figure 46 Wall  $y^+$  over blade surface for Mesh M2**

Data has been sampled along a series of sampling curves over the blade surface and along vertical lines at three locations selected to provide insight in the wall normal boundary layer profiles. All sampling locations are shown in Figure 47.

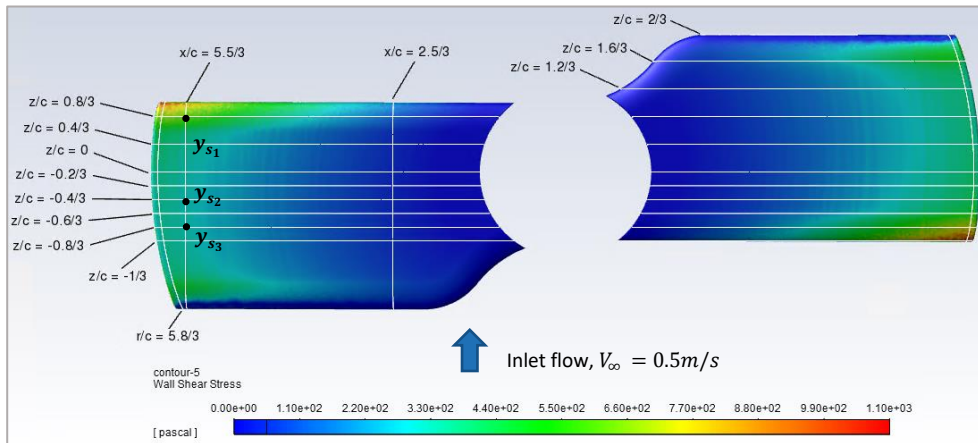


**Figure 47 Top view (from positive  $y$  direction) of turbine blades at initial time showing sampling lines. The vertical sampling lines  $y_{s_{1,2,3}}$  are shown as black dots at the intersections between  $x/c = 5.5/3$  and  $z/c = [0.8/3, -0.4/3, -0.8/3]$ . The initial blade position has leading edge aligned with  $x$  direction. The surface colouring refers wall shear stress predicted with Mesh M2.**

The boundary layer development along the sampling curve  $x/c = 5.5/3$  is considered first to assess whether the flow is similar to flow over a flat surface and to provide some measure of validation of the computational predictions. Figure 48 compares the velocity profile with the log law for flow over flat surfaces in the overlap part of the inner boundary layer region for the two meshes. These results are in line with predictions achieved with the  $k-\omega$  SST model with a  $y^+ \sim 10$  resolution of the boundary layer detailed in [23]. The profile slope is over-predicted but does generally follow the logarithmic law for sampling points at  $z/c = -0.4/3$  and  $z/c = -0.8/3$ . The finer mesh M1 shows a poorer fit which can be linked to local variations in the wall shear stress. The reasonable fit with the law of the wall suggests that sufficiently far from the curved leading-edge profile, the flow can be expected to recover characteristics of flow over flat surfaces. At  $z/c = 0.8/3$ , the proximity to the curved leading edge located at  $x/c = 1/3$  induces significant flow acceleration and pressure gradients. It is shown here to affect the extent of the logarithmic region with a boundary layer much thinner than would be expected with a zero gradient pressure profile. This can be seen from the plots of Figure 49. Approximations of the boundary layer thickness at the three sampling locations are compared to fully turbulent flat plate correlation estimates in Table 3. Not surprisingly there are significant differences near the leading edge but comparison is reasonable at sampling lines  $y_{s_2}$  and  $y_{s_3}$ , some evidence of convergence towards the flat plate correlation results with mesh refinement.

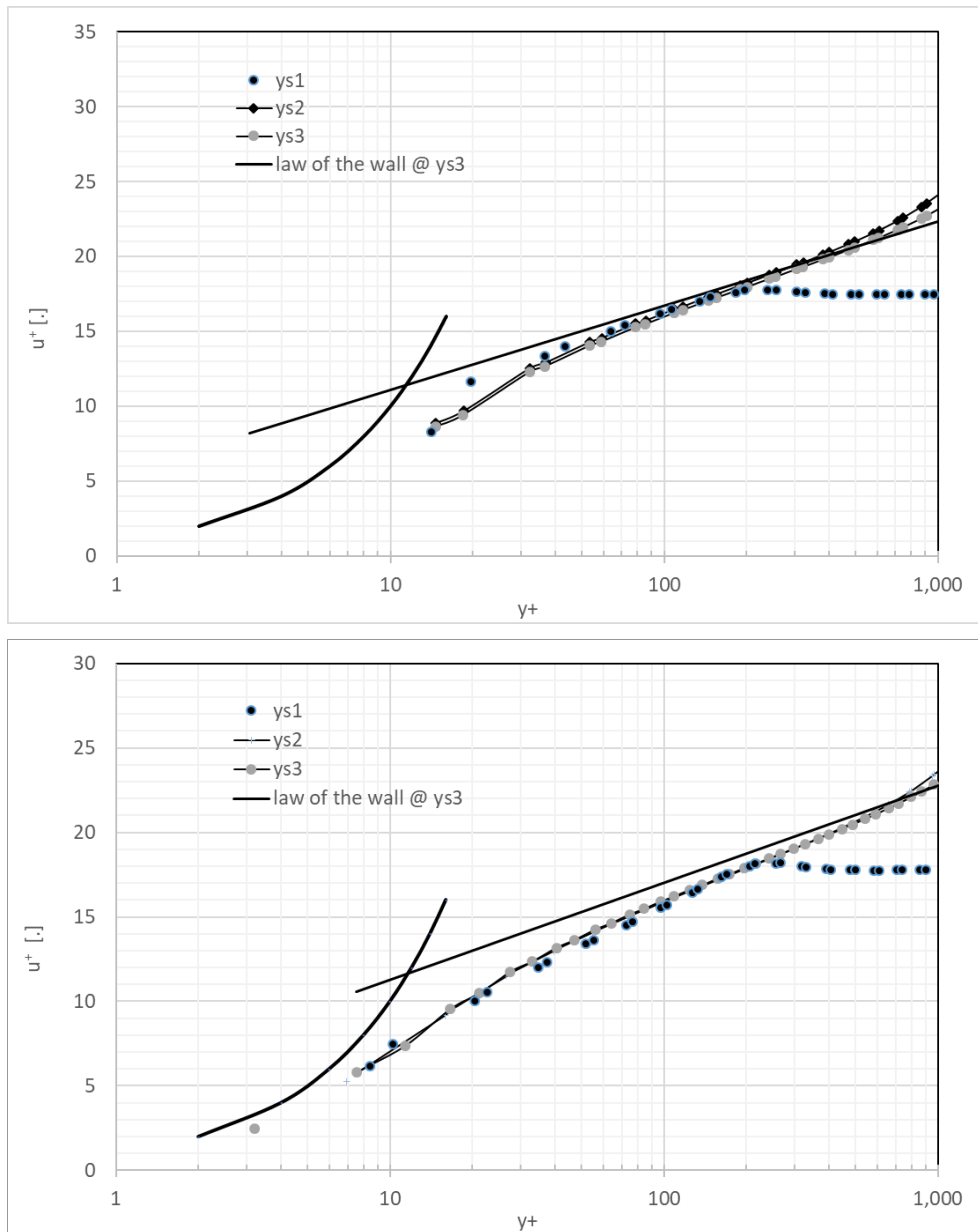
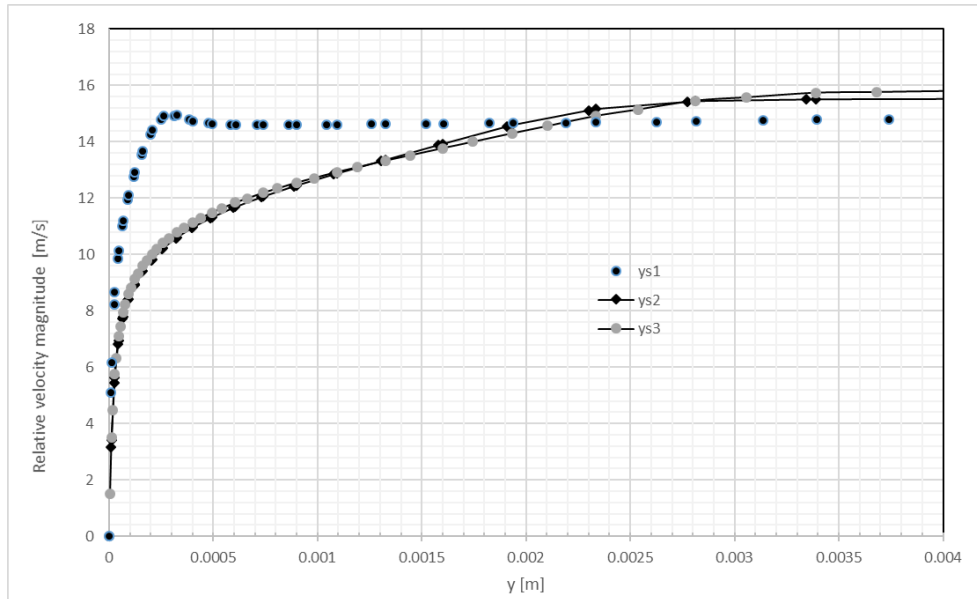


Figure 48 Velocity magnitude as function of wall distance in wall units over three vertical sampling lines  $y_{s1}$ ,  $y_{s2}$  and  $y_{s3}$ . [Top] Mesh M2 ( $y^+ \sim 12$ ). [Bottom] Mesh M1 ( $y^+ \sim 6$ )



**Figure 49** Velocity magnitude as function of wall distance over three vertical sampling lines  $y_{s1}$ ,  $y_{s2}$  and  $y_{s3}$  for mesh M1 ( $y^+ \sim 6$ ).

**Table 3** Boundary layer thickness compared to flat plate boundary layer correlations assuming a kinematic viscosity  $\nu = 10^{-6} \text{ m}^2 \cdot \text{s}^{-1}$

	Sample line $y_{s1}$	Sample line $y_{s2}$	Sample line $y_{s3}$
Flat plate correlation $\delta = 0.37xRe_x^{-1/5}$	$\delta = 0.000677m$ $Re_x = 3.98 \times 10^5$	$\delta_{fp} = 0.00277m$ $Re_x = 2.34 \times 10^6$	$\delta_{fp} = 0.00308m$ $Re_x = 2.68 \times 10^6$
$k-\omega$ SST prediction - M1	$\delta_{k-\omega} = 0.000249m$	$\delta_{k-\omega} = 0.0026m$	$\delta_{k-\omega} = 0.0032m$
$k-\omega$ SST prediction - M2	$\delta_{k-\omega} = 0.00026m$	$\delta_{k-\omega} = 0.0028m$	$\delta_{k-\omega} = 0.0036m$

The streamline plot of Figure 50 also indicates that the radial component of flow induced by centrifugal forces is small. Closer examination of the flow over the curved part of the leading edge does show a significant radial component but the effect is localised and confined to the part of blade leading edge with significant curvature.

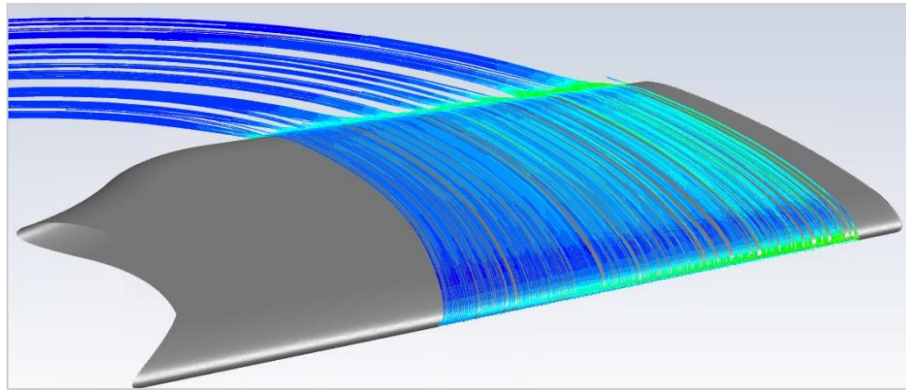


**Figure 50 Streamlines originating from seed line parallel and upstream of the leading edge.**

Achieving dynamic similarity of flow conditions between the current biofouling test turbine and the Nemmo turbine is neither needed nor possible given the difference in blade geometry. The purpose of the present real sea rig is to expose the textured surfaces and biofilms to hydrodynamic stresses that are representative of real operational conditions. This means essentially reproducing wall shear stresses of a similar magnitude at similar turbulent Reynolds numbers. If wall stresses are of similar magnitude, the viscous unit which scales the inner part of the boundary layer will be similar. If the Reynolds numbers are also similar the turbulent structures in the outer layer can be expected to have similar scales. Under such conditions, the micro-structures and micro-organisms which will be located in the inner part of the boundary layer can be expected to be exposed to similar turbulent structures and stresses. The flow Reynolds number calculated with the blade chord length as the length scale is  $Re_c = 8.9 \times 10^6$ , whereas the current turbine conditions along the sampling line  $x/c = 5.5/3$ , can be approximated as  $Re_c \sim 5 \times 10^6$ . This means a lower  $Re$  but a similar order of magnitude which will ensure similar turbulent structures. The next part of the present discussion aims to quantify the shear stress distribution over the test surface. This analysis is based on a comparison with conditions over the Nemmo blade section at radial position  $r = 8\text{ m}$  as predicted by the transitional  $k-\omega$  turbulence model from a 2D model with full resolution of the boundary layer down to the viscous sub-layer. Predicted wall shear stresses are shown in Figure 51 for a range of inlet turbulence from very low controlled level to realistic real seas conditions. The lower inlet turbulence simulations reproduce trends in the wall shear stresses that are consistent with transitional flow with a marked increase some distance from the leading edge. At the highest inlet turbulence, transition is no longer apparent, indicating that fully turbulent conditions develop on both sides of the airfoil generating higher stresses. There are notable differences between the suction and pressure sides of the airfoil. On the pressure side, the wall stresses are typically between  $110\text{ Pa}$  and  $500\text{ Pa}$  with turbulent transition at approximately delayed as far as 33% of the chord length. On the suction side the stresses cover a larger range reaching up to  $1000\text{ Pa}$  with an earlier transition.

By comparison the stresses along pseudo-radial sampling curves over the biofouling test blades vary in proportion to the radial position from the turbine centre of rotation. They are shown in Figure 52 to increase up to approximately  $500 - 510\text{ Pa}$  over the flat part of the turbine and up to  $800\text{ Pa}$  over the part of the sampling lines  $z/c = \pm 0.8/3$  which are adjacent to the blade leading edge ( $x < 0$  with  $z/c = -0.8/3$  and  $x > 0$  with  $z/c = 0.8/3$ ). It is interesting to note the sharp increase in stress in the latter case as the transitional model captures transition from laminar flow at approximately  $x \approx \pm 0.5$ .

These results were obtained with a low resolution of the viscous sublayer in particular towards the outer part of the turbine with a maximum  $y^+$  of approximately 6 for mesh M1. The  $k-\omega$  SST model is known to underestimate the wall stress in zero pressure gradient boundary layer flow by

approximately 6% at  $y^+=5$  and up to 40% at  $y^+ = 10$ . Comparing predictions with estimates from a fully turbulent flat plate correlation for the coefficient of friction  $C_f = 0.0592Re_x^{-0.2}$  provides some measure of this error with the present mesh. The stress distributions of Figure 53 use the length of the curved streamlines shown in Figure 50, assuming perfect circular paths, to determine the characteristic length for  $Re_x$  needed for the coefficient of friction. The comparison confirms that predicted stresses resemble distributions from zero pressure gradient planar flow. Simulated stresses are also shown to be lower than flat plate estimates. The maximum stress from the flat plate correlation is 30% and 25% higher than the simulated result at the blade tip for meshes M2 and M1 respectively but this reduces gradually towards the blade root. The mesh refinement has improved the comparison with the correlation in particular for  $x < 0$  that is for the part of the sampling line which lies closer to the leading edge. In this case and for a radial position up to 75% of the blade radius, the relative difference is in low single digit values.

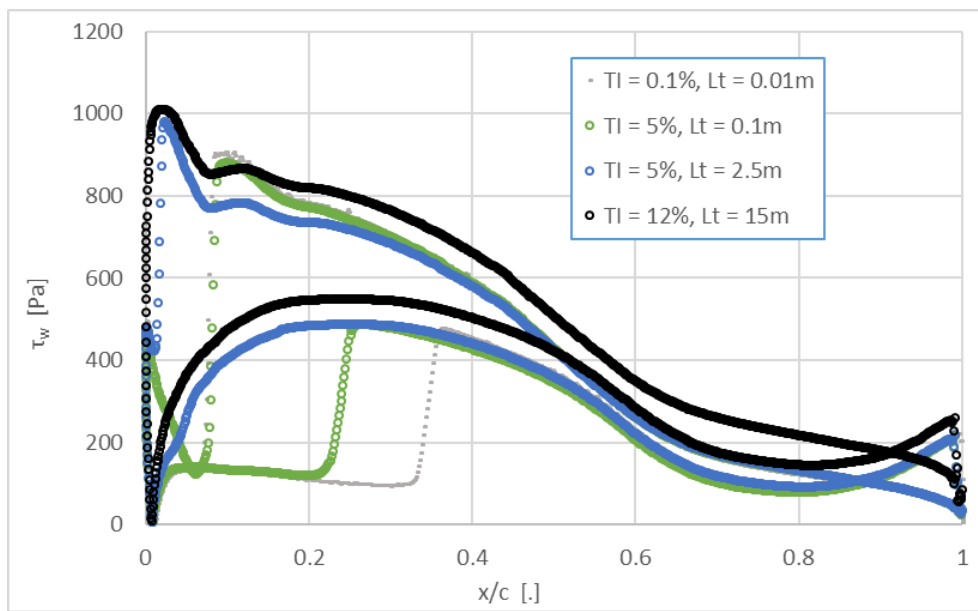


**Figure 51 Wall shear stress over the Nemmo blade section at  $r = 8\text{ m}$  from transitional turbulence model**

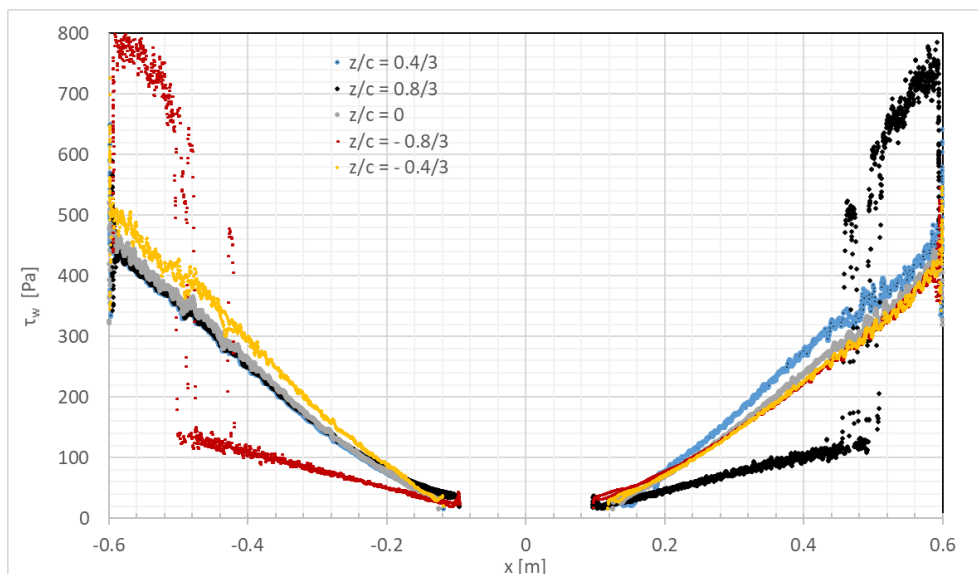


**Figure 52 Wall shear stress over the turbine blade from the real sea biofouling rig along five pseudo-radial sampling curves for Mesh M1.**

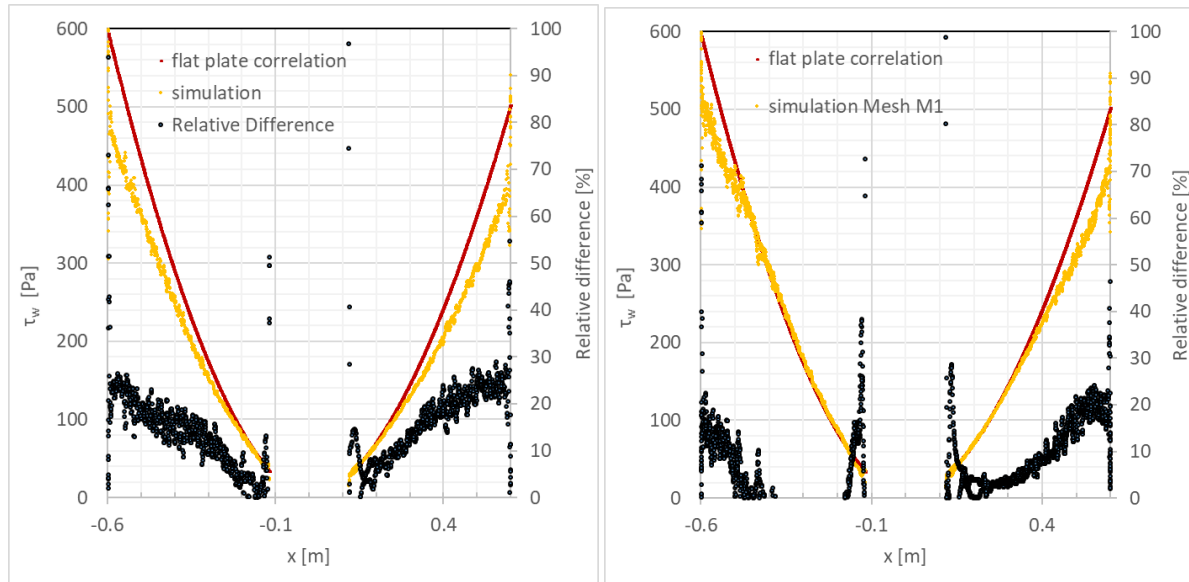


**Figure 53 Comparison between wall shear stress predictions from fully turbulent flat plate correlation and simulations along sampling curve  $z/c = -0.4/3$ . The relative difference between the simulated and the correlated predictions is shown on the secondary vertical axis as a percentage. [Left] Mesh M2. [Right] Mesh M1.**

### Test section dimensioning

Biofouling tests will involve comparing the dynamics of biofouling over a textured surface and a reference smooth surface both exposed to stresses in the marine environment. Simulation results indicate that a flat section of the biofouling turbine will be exposed to stresses reaching up to at least  $460 \text{ Pa}$  towards the blade tip and as much as  $750 - 800 \text{ Pa}$  close to the leading edge. These results confirm that the full range of stress predicted over the pressure side of the Nemmo blade section S9 can be reproduced. The higher stresses expected over the first 20% to 40% forward part of the blade on the suction side will not be recreated. The system has been designed to allow for higher rotational speed and increase the stress as required. The single-phase incompressible flow simulation indicate however that any increase will risk exposing the blade to cavitation. The biofouling turbine will be designed to allow insertion of two flat samples, one on upper surface of each of the two blades.

On the Nemmo blade, stresses are shown to depend significantly on the streamwise position as the flow transits to turbulence or as pressure gradients change with surface curvature. Once the flow has transitioned, the stresses show limited variations in the streamwise direction which suggests that it may be sufficient to use a sample surface with a width (in the streamwise direction) which does not extend the full chord length tested. The question is to decide whether the effects of boundary layer growth on the turbulent processes should be considered. A  $2 \text{ cm}$  wide section would see variations of approximately 6% in the stress along the circumferential direction at the tip of the blade (see Figure 54) and approximately 11% in the boundary layer thickness. This can be expected to have an impact on the biofouling organisms as they settle and grow. Although this effect is difficult to quantify from the present analysis, the design must make allowance for it. It is for this reason that a relatively large revised chord of  $c_f = 0.2$  will be used in the final design, giving  $Re_{c_f} \sim 3.3 \times 10^6$ . The section of the blade where biofouling will be investigated will extend between the sampling curves  $z/c = -0.6/3$ ,

$z/c = 0.6/3$ ,  $x/c = 2.1/3$  and  $x/c = 5.5/3$ . The rectangular section will be 12 cm wide and 34 cm long. It will be exposed to stresses ranging from approximately 110 Pa to 520 Pa (based on simulation results).

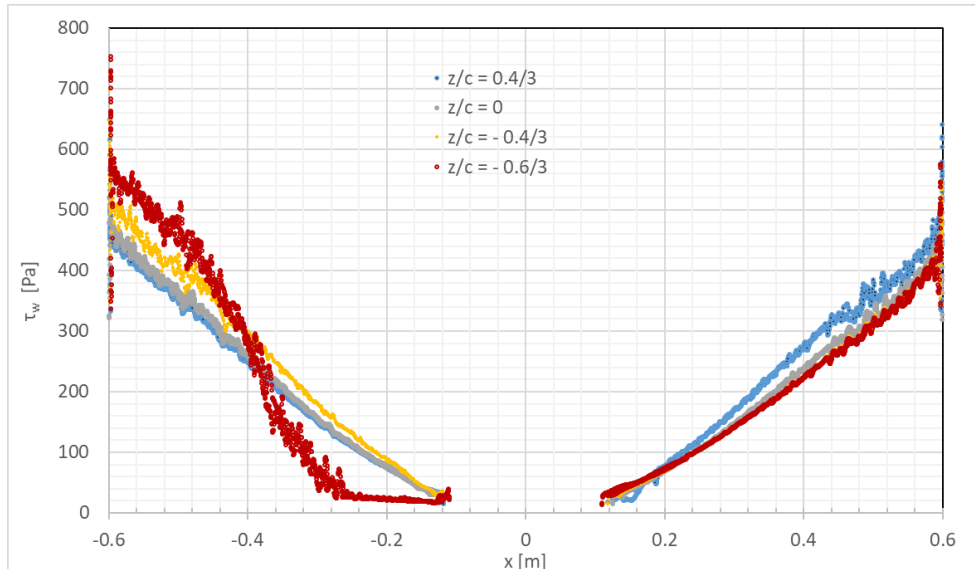


**Figure 54 Wall stresses distributions over 8 cm wide section bounded by  $z/c = \pm 0.4/3$**

The final design retained an incorporated in platform shown in Figure 43, is a slightly modified form of the blade shown in Figure 44, whereby the fore and aft asymmetry has been removed to remove unnecessary mass.

### Best performing candidate anti-fouling surface and material solutions

Three candidate anti-fouling solutions will be tested, and their performance assessed against a control smooth flat surface made from the original Magallanes composite material formulation. The three candidate anti-fouling solution were identified in Work Package 3. Their characteristics are summarised below:

1. Raised elongated rectangular blocks mimicking the micro ridges of brill fish, *Scophthalmus rhombus*, etched into the gel coat of the original Magallanes composite blade.
2. Smooth surface made with modified gel coat incorporating biocide nanoparticles.
3. Raised elongated rectangular blocks mimicking the micro ridges of brill fish, *Scophthalmus rhombus*, etched into the gel coat which incorporates the biocide nanoparticles.

### Test Programme

The purpose of the test campaign is to investigate the best performing biomimetic and multi-material solutions in a real sea environment over a 3-month period at a harbour site in the Irish Sea. The chosen micro-textures (detailed above) will be assessed on a fortnightly – monthly basis, with performance analysed against a control surface. Two methods have been proposed for the assessment of the anti-fouling solutions. These are summarized below:

**Visual Inspection** – A visual inspection of the candidate micro-textures will be performed on a weekly – fortnightly basis over a period of two months, with images being taken on a Nikon Digital Camera D3200 with AF-S MICRO NIKKOR 105 mm lens (3.5  $\mu\text{m}$  resolution). The most commonly found micro-organisms adhering to the surface will be identified from the series of images taken each month.

Each month, one section of the full-scale blade material will be taken back to the laboratory for biofouling characterization using a series of biochemical assays as described below. Biofilm will be extracted by either using adhesive tape, (i.e., Gorilla Glue White Duct Tape, 8.2 m x 48 mm) commonly used in forensic analysis [24], [25] and or by using a brushing technique to carefully extract the biofilm from the surface.

**Assays** – Biofilm will be characterized using a series of biochemical assays (i.e., Lowry protein assay, Anthrone-sulphuric acid assay) and scanning electron microscopy (SEM).

### Test Methodology

Biofilm will be characterized using a series of biochemical assays as identified in Work Package 3 (WP3) which are summarized below. The assays identified below will be used in Month 3 (M3) of the deployment campaign. During Months 1 – 3 (M1 – M3), visual inspection of the candidate micro-textures will be carried out every 1 to 2 weeks. Images will be taken on a Nikon Digital Camera D3200 with AF-S MICRO NIKKOR 105 mm lens (3.5  $\mu\text{m}$  resolution) to determine the type of organisms adhering to the surface of the micro-textures.

#### Lowry assay

The concentration of protein present in the biofilm will be determined using the Lowry Protein Assay, Peterson’s modification (Total Protein Kit, Micro Lowry, Sigma-Aldrich, Ireland). The protocol for the Lowry assay is summarized as follows [26];

- i. A 1 mL quantity of each unknown solution, and a blank is taken. 1 mL of Lowry reagent is added to each sample solution and control.
- ii. The solution is mixed using a vortex, and left to react at room temperature for 20 min.
- iii. A 0.5 mL aliquot of Folin & Ciocalteu’s Phenol Reagent is added to each sample solution and control.
- iv. Again, the solution is thoroughly mixed using a vortex.

The solutions are allowed to stand for 30 min at room temperature, before the absorbance is read using a UV-Vis spectrophotometer at 750 nm.

#### Anthrone-sulphuric acid assay for carbohydrate determination

The concentration of carbohydrate present in biofilm samples each month will be determined using the Anthrone-sulphuric Acid Assay. The protocol for the Anthrone-sulphuric Acid Assay is described below [21];

- i. A 100 mL solution of concentrated  $\text{H}_2\text{SO}_4$  (98 %) is chilled in an ice bath for 20 min.
- ii. A 0.2 % (w/v) Anthrone-sulphuric acid solution is prepared by adding an appropriate amount of Anthrone ACS Reagent (97 %) to the chilled  $\text{H}_2\text{SO}_4$  (98 %) solution.

- iii. A 2 mL volume of Anthrone-sulphuric acid solution is added to test tube containing unknown biofilm sample solutions.
- iv. The solutions are left to incubate for 15 min at 95 °C, taking care not to heat samples above 100 °C.

The solutions are then allowed to cool down to room temperature for 30 min, and absorbance is measured at 625 nm.

#### **Identification of diatom communities using scanning electron microscopy (SEM)**

The diversity of both microfouling (i.e., bacteria, diatoms), and macrofouling (i.e., barnacles, mussels) communities settling on the candidate micro-textures will be identified using scanning electron microscopy (SEM). Biofilm will be prepared for SEM, by fixation on a glass microscope slide using a glutaraldehyde solution and dehydration in methanol series (i.e., 0 – 100 %). Biofilm samples will be gold-coated using an Au-sputter coater (Edwards, U.K.) for 15 seconds and are observed under SEM using an accelerating voltage between 5 kV – 20 kV and a working distance of 8 mm.

### **Task 2.4.3 Definition of a tailored accelerated wear test for composite tidal blades working under cavitation turbulence and laminar flow conditions**

Evaluation of new materials or surface coatings for their resistance to cavitation erosion requires addressing both the intensity of the cavitation and the resistance of the material. In the absence of data of the performance for a new material in the cavitation flow field, experimental studies in laboratory offer a possibility to assess the cavitation erosion resistance. The laboratory tests aim at evaluating the resistance to cavitation erosion within a relative short time frame, whereas in the real field cavitation erosion may occur after long time exposure. Thus, we can mimic the material loss observed in full-scale by exposing the same material to cavitation erosion for a certain time in laboratory. This sample can then be used as a reference and other materials and coatings can be evaluated relative to the reference material.

There are various methods and devices to achieve cavitation erosion in a laboratory. In this project, an ultrasonic vibration apparatus, called “sonotrode” will be used. This method is standardized in ASTM G32 [27]. The cavitation is generated by a vibratory device employing a magnetostrictive ultrasonic horn. The high frequency oscillations induce formation of high and low pressures, which cause formation and collapse of cavitation bubbles. In ASTM G32-09, the vibration frequency is specified to 20 kHz and the peak-to-peak amplitude to 50  $\mu\text{m}$ . In the direct method, the sample is attached to the horn. ASTM G32 specifies a sample diameter of 16 mm. In the indirect (alternative) method, a stationary material sample is placed at a small distance below the vibrating horn tip made of a cavitation erosion resistant material. The indirect method is useful for testing materials that cannot easily be manufactured in a threaded button. The Figure 55 shows an example of the indirect set-up.

The conventional test procedure is to expose the sample to cavitation for a certain time, interrupt the test and record the weight. The sample is then returned to the same position for additional periods of exposure. Thus, the weight loss as a function of time can be calculated. Other erosion characteristics such as erosion imprint and width can be recorded and documented by photographs showing the erosion development as a function of time. The Figure 56 shows paint wear on samples after various time of exposure.

Erosion tests using ultrasonic cavitation provide reproducible cavitation in laboratory, but the cavitation is different from that on a turbine. The ultrasonic cavitation bubbles are nearly uniform sizes, at the same location and are excited at a fixed frequency. Real cavitation fields (e.g. on a turbine) have a distribution of bubble sizes and forms and have different exciting frequencies. In real cavitation the liquid flow field will interact with the bubbles which e.g. make them break-up in smaller sub-cavities or capture the bubbles in turbulent vortices.

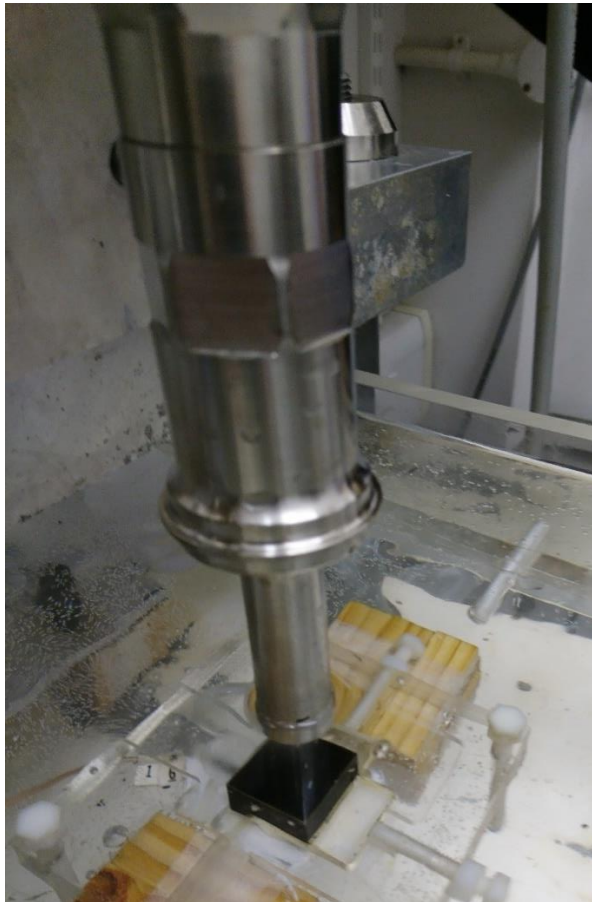


**Figure 55: An example of the indirect set-up of the sonotrode. A stationary material sample is placed at a small distance below the vibrating horn tip.**

Assessments of the risk for cavitation erosion on ship propellers is presently based on two types of tests performed in a cavitation tunnel: visual observations of cavitation and erosion tests using a soft paint technique. At model-scale testing with the propeller behind a complete ship model the conditions are typically such that the cavitation is not erosive enough to result in erosion of the propeller material. The reason for this is mainly the low water velocity that must be used to fulfil the hydrodynamic similarity laws to get the correct cavitation. Due to the low velocity the kinetic energy of the cavity collapses becomes too low to cause material damage. The material erosion is instead mimicked by the wear of the soft paint applied to the propeller at the standard erosion test. Assessments of the risk for cavitation erosion by observations is applicable also for tidal turbines, but we lack data of the statistical correlation between real erosion in full-scale and paint wear in model-scale for tidal turbines. Thus, we do not know if the the standard SSPA soft paint method will be applicable for assessment of cavitation erosion to the NEMMO turbine.

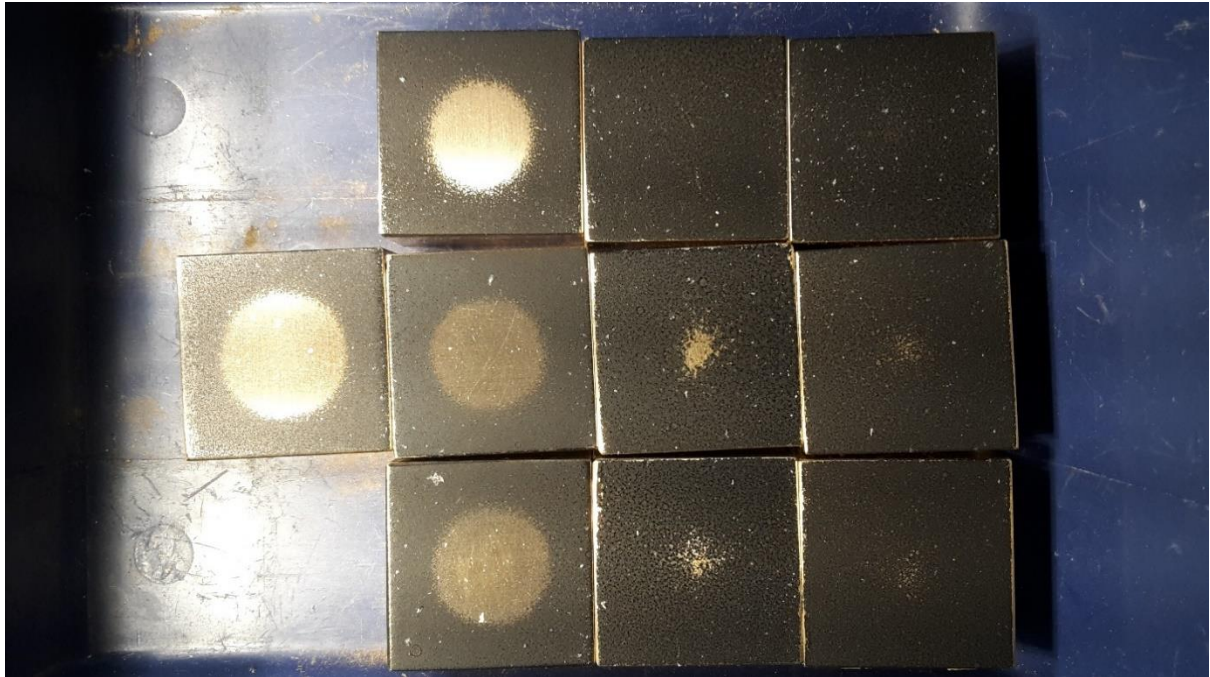


**Figure 56: Paint wear on samples after various time of exposure using the indirect set-up of the sonotrode**

## Task 2.4.4 Definition of an accurate dynamic test for fatigue evaluation of composite blades for tidal turbines

### Background information:

Wind turbine blades are being subjected to fatigue testing as part of the mandatory tests for type certification. These tests have been performed since the 1980's. The standard test method used by all test centres is the so-called resonance testing where the blade is excited in a cyclic testing with a frequency near the system eigen frequency. In this method the weight and inertia of the blade is used to generate the loading. This test method is used because it provides a number of advantages:

- Minimum excitation force input required
- Minimum power input required
- Relatively high and acceptable test frequency achieved (typically 0.4-1.0 Hz on a 60-80 m blade)



**Figure 57: Fatigue testing of wind turbine blades (Source: LM Wind Power)**

Tidal turbine blades are much shorter (5-10 m length) and designed for much higher fluid density. Water density is about 800 times higher than the normal air density. Therefore, the tidal blade design is much more solid, and the natural frequency of the blades is substantially higher than for wind turbine blades.

Previous tests on tidal blades have been performed using the so-called forced displacement method, where the blade is loaded at a number of loading points typically by means of hydraulic cylinders. Each half load cycle requires pressure application and subsequent pressure relief. This method has the advantage of individual control of each load station and full control on the loading speed.



**Figure 58: Traditional testing of tidal blades**

Other tidal turbine projects have concluded that resonance testing of tidal blades will not be possible, because the system eigen frequency will be too high (in the 10 Hz range). Such frequencies will result in undesired temperature raise in the blade material.

### The NEMMO project idea:

With the high system eigen frequency being the problem, the intention is to lower this frequency to an acceptable level by means of a flexible support between the blade and the test rig, eg between the test rig and the strong floor which it is connected to.

A lower test frequency will lead to less heat generation inside the blade material. The test frequency, still being rather high, will ensure fast performing of the test campaign, while at the same time allow for any stops necessary to cool down the blade material.

The aim is to design the entire set-up and perform trial tests to evaluate the performance and benefits / challenges related to the new test method.

An obvious advantage of this test method will be a much lower energy consumption, which is of particular interest considering the currently very high energy prices.

The expected output of the task was limited due to unexpected severe challenges. This is caused by mainly three issues:

1. The development of the structural fatigue loads (task 1.4) serving as input for this task could not been performed to an extent where the loads might be used for the specification of a fatigue test replicating real life operational conditions.
2. Due to a complicated blade design process with several iterations, the structural design data for the blade (such as stiffness matrix and weight distribution) is still not yet available.

3. The manufacturing of test blades is delayed due to the delayed design process.

The importance and the complexity of generating the overall structural design loads for the entire machine under given operational and extreme conditions have been underestimated in the project. Hence, no project partner is able to perform this task. Now, the intention is to generate a set of estimated fatigue loads based on the available static loads and the experience from the wind energy business about the relation between static extreme loads and fatigue loads. This will be a rather uncertain approach, but the best possible solution with the resources available.

Simulations are being performed with the purpose of defining a possible test set-up giving a reduced test frequency. Assuming this set-up, it will be evaluated if the set-up allows for an acceptable heating up of the blade material. A positive conclusion will be followed by trial tests in the Blaest test laboratory during 2023. This is subject to a test blade being available by then.

## Bibliography

- [1] N. Tual, N. Carrere, P. Davies, T. Bonnemains, and E. Lolive, "Characterization of sea water ageing effects on mechanical properties of carbon/epoxy composites for tidal turbine blades," *Composites Part A: Applied Science and Manufacturing*, vol. 78, pp. 380–389, 2015, doi: 10.1016/j.compositesa.2015.08.035.
- [2] J. Summerscales, *Durability of composites in the marine environment*, vol. 208. 2014. doi: 10.1007/978-94-007-7417-9\_1.
- [3] G. Youssef, S. Fréour, and F. Jacquemin, "Stress-dependent Moisture Diffusion in Composite Materials," *Journal of Composite Materials*, vol. 43, no. 15, pp. 1621–1637, 2009, doi: 10.1177/0021998309339222.
- [4] I. Kafodya, G. Xian, and H. Li, "Durability study of pultruded CFRP plates immersed in water and seawater under sustained bending: Water uptake and effects on the mechanical properties," *Composites Part B: Engineering*, vol. 70, pp. 138–148, 2015, doi: 10.1016/j.compositesb.2014.10.034.
- [5] M. Tedetti and R. Sempéré, "Penetration of Ultraviolet Radiation in the Marine Environment. A Review," *Photochemistry and Photobiology*, vol. 82, no. 2, pp. 389–397, 2006, doi: <https://doi.org/10.1562/2005-11-09-IR-733>.
- [6] B. Rånby, "Photodegradation and photo-oxidation of synthetic polymers," *Journal of Analytical and Applied Pyrolysis*, vol. 15, pp. 237–247, Mar. 1989, doi: 10.1016/0165-2370(89)85037-5.
- [7] G. E. Sheldrick and O. Vogl, "Induced photodegradation of styrene polymers: A survey," *Polymer Engineering & Science*, vol. 16, no. 2, pp. 65–73, 1976, doi: <https://doi.org/10.1002/pen.760160202>.
- [8] B. Singh and N. Sharma, "Mechanistic implications of plastic degradation," *Polymer Degradation and Stability*, vol. 93, no. 3, pp. 561–584, Mar. 2008, doi: 10.1016/j.polymdegradstab.2007.11.008.
- [9] "Home - HarshLab." <https://harshlab.eu/> (accessed Jun. 03, 2021).
- [10] "Estación Océano-Metereológica de Pasaia - AZTI," *Estación Océano-Metereológica de Pasaia - AZTI*. <https://estacion.euskoos.eus/> (accessed Jun. 03, 2021).
- [11] "RIM 21(4): Guide for the evaluation of biofouling formation in the marine environment," *RIM ∴ Revista de Investigación Marina by AZTI*, Nov. 07, 2014. <https://www.azti.es/rim/rim-214-guide-for-the-evaluation-of-biofouling-formation-in-the-marine-environment/?lang=en> (accessed Jun. 03, 2021).
- [12] D. Choqueuse, P. Davies, F. Mazéas, and R. Baizeau, "Aging of Composites in Water: Comparison of Five Materials in Terms of Absorption Kinetics and Evolution of Mechanical Properties," *High Temperature and Environmental Effects on Polymeric Composites: 2nd Volume*, pp. 73-73–24, 2009, doi: 10.1520/stp11369s.
- [13] "ASTM F1980-02 Standard Guide for Accelerated Aging of Sterile Medical Device Packages," vol. 11. pp. 1–6, 2002. doi: 10.1520/D7102-10.Copyright.
- [14] P. Davies, "Environmental degradation of composites for marine structures: New materials and new applications," *Philosophical Transactions of the Royal Society A: Mathematical, Physical and Engineering Sciences*, vol. 374, no. 2071, 2016, doi: 10.1098/rsta.2015.0272.

- [15] T. Kumar, BG., Singh, RP., Nakamura, “Degradation of Carbon Fiber-reinforced Epoxy Composites by Ultraviolet Radiation and Condensation,” *Journal of Composite Materials*, vol. 36, no. 24, pp. 2713–2733, 2002, doi: 10.1106/002199802028682.
- [16] D19 Committee, “Practice for the Preparation of Substitute Ocean Water,” ASTM International. doi: 10.1520/D1141-98R13.
- [17] “ASTM D5229 Standard Test Method for Moisture Absorption Properties and Equilibrium Conditioning of Polymer Matrix Composite Materials,” p. 1, doi: 10.1520/D5229.
- [18] “ASTM D3039, Standard Test Method for Tensile Properties of Polymer Matrix Composite Materials.” pp. 1–13, 2014. doi: 10.1520/D3039.
- [19] “ASTM D5379 Shear Properties of Composite Materials by the V-Notched,” no. March, pp. 1–13, 2005, doi: 10.1520/D5379.
- [20] “ASTM D 7264 Standard test method for flexural properties of polymer matrix composite materials,” vol. 7, p. 11, 2007, doi: 10.1520/D7264.
- [21] E. C. P. Catão *et al.*, “Shear Stress as a Major Driver of Marine Biofilm Communities in the NW Mediterranean Sea,” *Front. Microbiol.*, vol. 10, 2019, doi: 10.3389/fmicb.2019.01768.
- [22] “ANSYS Fluent Theory Guide.” ANSYS, Inc., 2019.
- [23] R. H. Nichols, “Turbulence models and their application to complex flows,” *University of Alabama at Birmingham, Revision*, vol. 4, p. 89, 2010.
- [24] C. Forsberg, L. Jansson, R. Ansell, and J. Hedman, “High-throughput DNA extraction of forensic adhesive tapes,” *Forensic Science International: Genetics*, vol. 24, pp. 158–163, Sep. 2016, doi: 10.1016/j.fsigen.2016.06.004.
- [25] J. Gunnarsson, E. Helena, and R. Ansell, “Success rates of a forensic tape-lift method for DNA recovery,” *Problems of Forensic Sciences*, vol. LXXXIII, pp. 243–254, 2010.
- [26] C. Richards, N. O’Connor, D. Jose, A. Barrett, and F. Regan, “Selection and optimization of protein and carbohydrate assays for the characterization of marine biofouling,” *Anal. Methods*, vol. 12, no. 17, pp. 2228–2236, May 2020, doi: 10.1039/D0AY00272K.
- [27] G02 Committee, “ASTM G32-09, Test Method for Cavitation Erosion Using Vibratory Apparatus,” ASTM International. doi: 10.1520/G0032-10.

